RESEARCH AND DEVELOPMENT TECHNIQUE FOR ESTIMATING AIRFLOW AND DIFFUSION PARAMETERS IN CONNECTION WITH THE ATMOSPHERIC WATER RESOURCES PROGRAM

Interim Report

Prepared by

M. M. Orgill

Principal Investigator: J. E. Cermak
Co-Principal Investigator: L. O. Grant

Period September 2, 1970 to February 28, 1971
Atmospheric Water Resources Research
Bureau of Reclamation
Contract No. 14-06-0-6842

Fluid Dynamics and Diffusion Laboratory
College of Engineering
Colorado State University
Fort Collins, Colorado
80521

ABSTRACT

This report presents a summary of the research and tentative findings on the use of scaled topographic models and laboratory techniques to study the transport and dispersion of cloud seeding material over mountainous terrain. Three mountainous areas along the continental divide have been selected by the Bureau of Reclamation for such studies. Each area has cloud seeding programs in progress.

Keywords: Weather modification, cloud seeding, model studies, dispersion, boundary layers.

TABLE OF CONTENTS

Section		Page
	LIST OF FIGURES	iv
	LIST OF TABLES	vi
	LIST OF SYMBOLS	vii
I	INTRODUCTION	1
	Purpose of Research Program	1
	Research Goals	3
	Research Activities for the Period September 1970 - February 1971	5
II	REVIEW OF SIMILITUDE REQUIREMENTS	6
	General Similitude Requirements	6
	Laboratory Airflow Models	8
	1. Neutral airflow model	8
	2. Barostromatic airflow model	9
	Scale Distortion	9
III	SAN JUAN MOUNTAIN STUDY	11
	Field Data	12
	Design of Field Experimental Program	14
	1. Generator network	14
	2. Criteria for experimental day	15
	Laboratory Experiments	15
	1. Topographic model	15
	2. Boundary conditions	16
	3. Similitude conditions	17
	4. Wind velocity and turbulence profiles	18

TABLE OF CONTENTS - (Continued)

Section		Page
	5. Dispersion measurements	21
IV	ELK MOUNTAIN STUDY	27
	Field Data	28
	Laboratory Experiments	28
	Results	29
V	EAGLE RIVER VALLEY - CLIMAX STUDY	32
	Field Data	33
	Laboratory Experiments	35
VI	FUTURE WORK	36
	ACKNOWLEDGMENTS	37
	REFERENCES	38
	APPENDIX I	40
	TABLES	42
	FIGURES	46

LIST OF FIGURES

Figure		Page
1	Potential and Equivalent Potential Temperature and Horizontal Wind Distribution with Height at Durango, Colorado (April 22, 1970)	47
2	Location of Field Generator Sites that were Modeled for the San Juan Topographic Model	48
3	Types of Sources Designed and Utilized on the Model for Emitting Radioactive Gas	49
4	Schematic Diagrams of the Colorado State University Environmental Wind Tunnel and Upstream Boundary Conditions	50
5	Approach Velocity and Longitudinal Turbulence Profiles for the Roughness Upstream Conditions	51
6	Comparison of the Model Wind Velocity Profiles for Different Upstream Conditions and a Field Velocity Profile	52
7	Schematic Diagram of the Laboratory Equipment for Obtaining Average Longitudinal Velocities, Longitudinal and Lateral Turbulent Intensities	53
8	Vertical Cross-Sectional View of the Wind and Turbulence Fields over the Model	54
9	Components of Radioactive Gas Sampling System	55
10	Schematic Diagram of the Radioactive Gas Sampling System Showing Flow Direction During Sampling	56
11	Pictures Illustrating Meandering of the Smoke Plume with Time in the Wind Tunnel	57
12	Titanium Dioxide Deposit in the East and West Fork Valleys of the San Juan River Illustrating the Effects of Air-flow Separation	58

LIST OF FIGURES - (Continued)

Figure		Page
13	Ground Deposit as the Result of Chemical Smoke from Different Simulated Ground Sources	59
14	Distribution of the Nondimensionalized Concentration for Two Lateral Cross-Section Over the Model. Source: Pagosa Springs	60
15	Same as Figure 14. Source: Oak Brush Hill	61
16	Same as Figure 14. Source: Carracas Mesa	62
17	Distribution of Radioactive Gas Concentration Over Wolf Creek Pass Cross-Section as the Result of Multiple Sources	63
18	Same as Figure 17	64
19	Comparison of Surface Ground Concentration for Elk Mountain Model and Trajectories of Field Constant-Volume Balloons	65
20	Vertical Height Profile of Constant-Volume Balloon and Associated Temperature Conditions	66
21	Vertical Profiles of the Horizontal Velocity as Determined by the Smoke-Wire Equipment	67
22	Temperature Profiles Over the Elk Mountain Model	68
23	Potential and Equivalent Potential Temperature Profile at Camp Hale during Day of Aircraft Sampling	69
24	Constant-Volume Balloon Trajectory and Aircraft Sampling Track	70
25	Concentration Distribution of Silver-Iodide Over Three Different Regions of the Eagle River Valley-Climax Area	71

LIST OF TABLES

Table		Page
1	EG and G Project Generator Sites for the San Juan Mountain Area	43
2	Momentum Boundary Layer Thickness and Average Lateral and Longitudinal Turbulent Intensities Over the San Juan Topographic Model	44
3	Elk Mountain Study - Plume Axis Deflection from Free-Stream Direction	45

LIST OF SYMBOLS

Symbol	Definitions
$\bar{c}$	Average concentrations
c_p	Specific heat of constant pressure
$\mathcal{D}$	Depletion and deposition mechanisms acting on a tracer plume
Eu	Euler number
f	Coriolis parameter $2\Omega \sin \phi$
Fr	Froude number
g	Acceleration of gravity
H	Boundary layer thickness
h_s	Height of source above the ground
K_m	Coefficient of exchange of momentum
K_x , K_z	Coefficients of eddy viscosities in x and z directions
K	Constant eddy - diffusivity coefficient
k	Coefficient of thermal conductivity
L	Reference length
P	Pressure
Pe_t	Turbulent Péclet number
Pr_t	Turbulent Prandtl number
Q	Source strength; time rate of material emission from a continuous point source
Q_E	Latent heat of evaporation and evapotranspiration
Q_G	Transfer of heat through the ground
Q_H	Turbulent transfer of sensible heat to the atmosphere
$Q_{L\uparrow}$	Long-wave radiation emitted by the surface
$Q_{L\downarrow}$	Long-wave radiation received by the surface from the atmosphere

Symbol	Definitions
Q_R	Short-wave radiation reflected from the earth
Q_T	Short-wave radiation from sun and sky
Re_t	Turbulent Reynolds number
Ri	Richardson number
Ro	Rossby number
$\vec{r}$	Three-dimensional vector for position
T	Local temperature and travel time
T_s	Temperature of source material
t	Time
U	Reference or local velocity
$\overline{U}$	Mean wind speed
U_g	Freestream or geostrophic velocity
w_s	Source efflux velocity
X	Reference distance
$\vec{Z}$	Height of terrain; model or prototype
α	Index indicating degree of scale exaggeration
ε	Height of roughness features
θ	Potential temperature
μ	Coefficient of dynamic viscosity
ν	Coefficient of kinematic viscosity
ρ	Air density
$\frac{\sigma_i}{\overline{U}}$	Turbulent intensities for three-space dimensions
$)_m$	Pertains to model

Symbol	
$)_f$	Pertains to field
*	Characteristic variable, e.g., length, velocity, etc.

I. INTRODUCTION

Purpose of Research Program

Several weather modification field programs are now in progress to augment water resources in the western states by artificially seeding wintertime orographic cloud systems. Artificial ice nuclei in the form of silver-iodide smoke are released from ground-based and air-borne generators in the natural airstream where turbulence and convection currents are expected to carry the material into supercooled water clouds, and thus initiate precipitation by the Bergeron ice crystal process.

The physical basis for treating cold orographic clouds by seeding has been discussed by Bergeron [Ref. 2], Ludlam [Ref. 13] and Grant and colleagues [Ref. 8]. The orographic clouds which form along and windward of the mountain ranges over the western United States are frequently composed of supercooled liquid droplets. The temperature activation spectrum of natural nuclei is such that the number of effective natural ice nuclei does not meet cloud requirements, under some conditions, for converting the cloud water to ice form at the warmer cloud temperatures and higher condensation rates. In such cases snow may not develop, or the precipitation process may be inefficient.

If artificial ice nuclei can be activated in the saturated orographic stream far enough upwind of the mountain barrier, a more efficient conversion of cloud water to ice crystals should result in increased snowfall. Otherwise, the unconverted cloud water evaporates to the lee of the mountain barrier.

Successful cloud seeding depends upon the introduction of sufficient artificial nuclei (e.g., silver iodide) into supercooled clouds to obtain optimum crystal concentrations. If the concentration of crystals in the cloud should be less than the optimum concentration, then not all of the vapor provided by the orographic updraft can be readily condensed upon the snow crystals. When the concentration of crystals is above the optimum number overseeding may occur and the resultant precipitation may be less than would have occurred naturally.

Grant and colleagues [Ref. 8] have developed a simple model for showing the variation of optimum ice nuclei concentration as a function of cloud system temperatures. The optimum ice nuclei concentration was defined as that which enabled the cloud system to grow ice by diffusion at a given condensation rate. In the Climax, Colorado area, the optimum concentration of crystals needed to insure an efficient precipitation process was estimated between 100 to 5 per liter depending on the range of temperatures (-13°C to -35°C) and vertical velocities (1.5 to 0.1 m/s) that occur at this location. A more refined and improved model has been derived by Chappell [Ref. 4] that was tailored for existing cloud conditions at Climax and Wolf Creek Pass, Colorado.

The realization of the delivery of the optimal distribution of seeding material to orographic cloud systems presents a complex theoretical and operational problem. In order to help solve this complex problem several questions need to be answered in a quantitative manner. Such questions are:

1. Under given storm conditions will artifical freezing nuclei reach the target area?

2. How much of the target volume will be covered (i.e., horizontal and vertical dimensions of seeding plume) and in what concentrations?

3. What are the effects of stability, wind shear, orographic features and other natural factors on dispersion of the seeding material?

The overall purpose of this research is to help provide some answers for the above questions by utilizing the wind tunnel as a tool to model the atmospheric planetary boundary-layer over mountainous terrain and the transport-dispersion of a passive tracer material simulating the silver-iodide seeding material. A second phase of the research involves obtaining limited field data that will assist in enlarging our understanding of the transport-diffusion process in the field and also providing relevant data to check on the laboratory simulation results. The field program is limited to the Climax-Eagle River Valley area; the remainder of the field data for other areas will be provided by private contractors and the University of Wyoming Natural Resources Research Institute.

Research Goals

The wind tunnel or laboratory method consists of making concentration measurements of a dispersing tracer material over a scale model of selected terrain placed in a simulated atmospheric flow. Field measurements of tracer concentration for selected meteorological conditions are used to confirm and/or correct the laboratory results. The general objectives for the research are as follows:

1. Determine the full capability for laboratory simulation of airflow over complex roughness features.

2. Investigate the similarity for atmospheric transport and dispersion of particulate material such as silver iodide over complex terrain with a wind-tunnel model.

3. Evaluate the use of wind-tunnel simulation of airflow and transport in various types of orographic terrain as related to weather modification operations.

4. Obtain field information on the relative dispersion and transport characteristics of tracers with particle sizes ranging from meter to molecular sizes.

5. Establish modeling criteria for future operational programs in weather modification.

The more specific and intermediate objectives are described in the following sections. The objectives have been altered somewhat to include and place emphasis on the acquisition of information on plume characteristics for the San Juan Mountain areas during winter storms. This is in direct support of the pilot seeding project planned for the Colorado River Basin.

This report summarizes the research and results obtained during the past six months on three selected topographic regions where operational cloud seeding is in progress. These areas are:

1. Eagle River Valley-Climax area (Central Colorado)

2. Elk Mountain area (Wyoming) and

3. San Juan Mountain area (Southern Colorado).

Research Activities for the Period September 1970 - February 1971

Tentative results from each type of activity, as outlined under Research Goals, are summarized in separate sections. Section II gives a brief review of the research efforts toward evaluating the requirements of similarity between model and field parameters. The problem of similarity with a scaled distorted model is also considered because of the necessity of constructing the San Juan topographic model with a distorted vertical scale.

Section III discusses the present field data from the San Juan Mountain region and how these data will be utilized to assist the laboratory simulation program. The laboratory simulation is also summarized in this section. Experimental instrumentation, measurements and results are discussed in relation to studies with the San Juan topographic model. Some discussion is included on field and model comparisons.

Section IV discusses the laboratory activities for the Elk Mountain region of Wyoming. Section V reviews the activity on the Eagle River Valley - Climax study and presents part of the aircraft sampling data that has been obtained in the area this past year. Section VI outlines the plans for the remaining laboratory studies and field-data analysis.

II. REVIEW OF SIMILITUDE REQUIREMENTS

General Similitude Requirements

The purpose of this section is to present in brevity the research efforts toward evaluating the major requirements of similitude between field and models. Complete similarity between two flow systems of different length scales require geometrical, kinematical, dynamical and thermal similarity. In addition, certain boundary conditions should also be duplicated.

The following outline gives the general requirements necessary for complete flow similarity.

1. Boundary conditions
    a. Upstream conditions - initial velocity, turbulence, mean temperature profiles
    b. Upper-level flow conditions
    c. Lower boundary conditions - surface topography and temperatures
    d. Side boundary conditions - topography and wind-tunnel wall effects
2. Geometric similarity
    a. Modeling of terrain features, roughness, trees, etc.
    b. Boundary-layer thickness
3. Kinematic similarity
    a. Rossby number (Coriolis effects) equality
    b. Streamline similarity
    c. Velocity profile similarity

4. Dynamic similarity

   a. Reynolds number equality

   b. Péclet number equality

   c. Richardson or Froude number equality

   d. Prandtl number equality

   e. Euler number equality

5. Similarity of heat transfer from the surface boundary

   Exact similarity requires duplication of the various heat transfer variables expressed in the heat-transfer equation viz,

$$Q_T - Q_R + Q_{L\downarrow} - Q_{L\uparrow} = \pm Q_G \pm Q_H \pm Q_E \ . \qquad (2.1)$$

6. Similarity requirements for atmospheric transport and dispersion.

   Similarity between field and model requires identical spatial distributions of concentration. The problem is complex and requires duplicating the following variables of the actual atmosphere with a physical model:

$$\overline{C}\,(\vec{r}) = f(Q\ ,\ w_s\ ,\ T_s\ ,\ h_s\ ,\ \mathcal{D}\ ,\ \vec{Z}\ ,\ \varepsilon\ ,\ Ro\ ,\ Re_t\ ,$$
$$\sigma_i/\overline{U}\ ,\ Ri\ ,\ Pr_t\ ,\ Eu\ ,\ Pe_t\ ,\ t)\ . \qquad (2.2)$$

   The similitude parameters (Reynolds number, etc.) governing the airflow and dispersion patterns may be derived by dimensional analysis, similarity theory or inspectional analysis. No attempt will be made in this report to give a comprehensive description of each of these methods or the derivation to obtain the relevant similitude parameters.

Complete derivations may be found in various publications, such as, McVehil, et al., [Ref. 15], Nemoto [Ref. 16] and Cermak and Arya [Ref. 3]. Appendix I defines many of the relevant similitude parameters encountered in the present problem.

Laboratory Airflow Models

The physical limitations of the present laboratory experimental apparatus requires the relaxation of certain similitude requirements, thus, complete similitude between field and model cannot be totally satisfied. However, past studies have indicated that partial similarity may be adequate for obtaining reasonable results.

The following statements briefly summarizes the principal assumptions of the airflow models that have been used to obtain diffusion results to date:

1. Neutral airflow model

   a. Thermal similarity

$$\left.\frac{1}{\theta}\frac{\partial\theta}{\partial Z} \sim 0\right]_f \equiv \left. -\frac{1}{\rho}\frac{\partial\rho}{\partial Z} \sim 0\right]_m \qquad (2.3)$$

   b. Airflow and dispersion similarity

   The nondimensional concentration distribution at any point downstream from a source is assumed a function of the following variables,

$$\frac{\bar{C}\,\bar{U}\,h_s^2}{Q} = f\left(\frac{Z}{H},\ Re_t,\ U(z)/U_g,\ t/T\right) \qquad (2.4)$$

In this physical model the airflow is aerodynamically rough which allows relaxing the requirements of Reynolds number duplication [Refs. 20 and 18]. Usually the turbulent Reynolds or Peclet numbers cannot be checked because the data are not available.

2. Barostromatic airflow model

a. Thermal similarity

$$\left.\frac{1}{\theta}\frac{\partial\theta}{\partial Z} > 0\right)_f \equiv \left. -\frac{1}{\rho}\frac{\partial\rho}{\partial Z} > 0\right)_m \qquad (2.5)$$

b. Airflow and dispersion similarity

The nondimensionalized concentration distribution is assumed a function of the following variables,

$$\frac{\overline{C}\,\overline{U}\,h_s^2}{Q} = f\left(\frac{Z}{H}\,,\ Re\,,\ Ri\,,\ Pr\,,\ U(z)/U_g\,,\ t/T\right)\,. \qquad (2.6)$$

This type of airflow model was evaluated in the Eagle River Valley - Climax study [Ref. 18].

Scale Distortion

Distorted models are common in hydraulics and ocean engineering laboratory studies but have not been used to any great extent in wind-tunnel modeling. A recent study has examined the problem in relation to modeling urban areas [Ref. 6]. A complete examination of the similarity problem has not been considered, however, Nemoto [Ref. 16] has analyzed some aspects of the problem.

Nemoto has examined the equation of motions of a turbulent atmosphere and found that in case of vertical exaggeration the degree

of exaggeration is related to K_x and K_z, the eddy diffusion coefficients in the longitudinal and vertical directions. He found that the relation

$$\alpha = \left[\frac{\left(\frac{K_x}{K_z} \right)_f}{\left(\frac{K_x}{K_z} \right)_m} \right]^{1/2} \tag{2.7}$$

should be satisfied between α and the eddy diffusion coefficients for the mean flow patterns to be similar for prototype and model. At the present time the difficulty of obtaining measurements of the eddy diffusion coefficients in the field and model have hindered efforts to check this relation. However, recent efforts have been attempts to examine this relation in terms of a fully rough flow in the wind tunnel [Ref. 6].

SAN JUAN MOUNTAIN STUDY

Contributions by

F. Chaudhry

S. Nayak

K. Kitabayashi

R. Kahawita

W. Tully

III. SAN JUAN MOUNTAIN STUDY

Field Data

The available field data as acquired from Western Scientific Services, Inc., and EG & G was examined to obtain some information on the frequency of certain weather events that would be comparable to the model experiments. The information on hand is not extensive and not completely adequate for our purpose hence some of the conclusions or comparisons must be considered tentative until additional field data become available for the project.

Small samples of temperature and wind data were examined for the general area. Wind data were available from 15 Western Scientific Service's rawinsondes released from Durango and 13 pilot balloon releases from Chromo. Four pilot balloon releases from Pagosa Springs were obtained from EG & G.

One of the reasons for the small sample of data was that only soundings with southwest wind were requested since the present model only simulates the southwest flow direction.

An examination of these data along with wind studies conducted by EG & G [Ref. 7] reveals the following wind-pattern characteristics in this area:

1. According to EG & G studies, a thermal-tidal wind regime may exist between the lower-plateau areas to the southwest and the mountain massif of the Rockies to the north and east. This means that at night northwesterly or northerly wind components increase in the lower levels while during the day southwest or southerly components increase. In addition, a local scale upslope and downslope circulation driven by the

diurnal heating and cooling pattern of adjacent mountains and valleys has been observed from pilot balloon data. Such wind regimes are most evident in synoptically quiescent periods within the planetary boundary layer.

Such wind regimes should not pose any problem for the laboratory simulation since the wind regime of interest is large-scale storm-driven southwest winds where thermal-tidal and diurnal winds would only be minor modifications to the large-scale wind pattern.

2. Examination of the wind vertical profiles during deep southwest wind periods show that a variety of wind speed and direction profiles exist. However, there are periods during southwest winds when the wind direction varies little in direction within the geostrophic wind regions.

The wind data is not abundant enough to arrive at any figures on the frequency of these occasions but this is important information since the present model assumes that little turning of the wind occurs at the geostrophic heights or in the lower levels except that provided by topographic relief.

3. The rawinsonde data for Durango was listed by a special computer program for each day for the following variables: pressure, temperature, relative humidity, mixing ratio, potential temperature and equivalent potential temperature. A plot of the potential and equivalent potential temperature with height was made for each sounding.

Examination of the potential and equivalent potential-temperature profiles showed that the stability conditions may vary widely even during storm periods with precipitation. An important question regarding the stability is whether events with near-neutral stability

through a deep layer exists in this area. This is of importance since the present model experiments were conducted under the assumption that near-neutral conditions existed in the field.

Only one or two soundings showed these near-neutral characteristics and these were not ideal. Figure 1 shows the temperature and wind vertical profile for April 22, 1970 at 1700 MST. This sounding exhibited temperature conditions which the model experiments could approximate but further information is needed in order to determine how long such stability periods persist.

4. Studies by EG & G [Ref. 7] have found that during precipitation conditions, trapping low-level temperature inversions were virtually non-existent but during fair weather with strong long-wave radiational losses from snow cover an inversion was very predominant. This information is of importance since there was no attempt during these studies to model low-level temperature inversions.

Design of Field Experimental Program

1. Generator network

According to information published by EG & G [Ref. 7] the silver-iodide generator network consist of 33 ground-based generator sites. Of these, 20 will be manually operated and 13 will be remote-controlled. The location of the generators are based on the Colorado State University design study [Ref. 8] which specified a primary line of generators 20 - 25 miles from the main mountain massif, a secondary line 40 - 45 miles and several close-in generators.

2. Criteria for experimental day

An experimental day for seeding has been defined in terms of predicted precipitation, 500 mb temperatures and predicted 700 mb wind directions (toward the mountain slopes $\sim$ 150° through 300°). A preliminary study of the frequency of experimental days to be expected showed a variation from 2 to 10 experimental days per month (winter season) [Ref. 7].

Laboratory Experiments

1. Topographic model

The construction of the San Juan model was described in the Annual Report [Ref. 19] and details of this work will not be repeated in this report.

The model was constructed to simulate a south-southwest ($\sim$ 220°) freestream or geostrophic wind. The large extent of the geographical area to be modeled required distorting the model in the vertical scale. The scales were 1:14,000 for the horizontal and 1:9,600 for the vertical.

The topographic model only covers part of the area of the field generator network. Figure 2 and Table 1 shows the number of generator sites simulated on the topographic model. Fifteen of the 33 field generator sites were constructed on the model. In addition, eight other sites were constructed for optional measurements.

Two different types of sources were designed for the model as shown in Fig. 3. Type I was used principally for the present experiments for neutral flow with the exception of the three

sources located several feet from the mountain massif. In this case, Type II was utilized in the experiments.

The disparity in size of field and model sources can not be resolved due to the scale of the model, but the characteristics of the sources (w_s , T_s , h_s) are assumed to be lost as turbulent mixing takes place downstream from the sources.

2. Boundary conditions

In order to approximate the velocity profiles and turbulence the upstream section of the wind tunnel had to be modified with artificial devices. Figure 4 shows a schematic diagram of the Colorado State University environmental wind tunnel and the present upstream modifications. At the beginning of the test section two sets of cardboard tubes were fixed into place, the first set, 36 in. long and 2 1/2 in. diameter were placed on the floor with the second set, 18 in. long and 2 1/2 in. diameter placed on top of the first.

Downstream from the tubes small gravel roughness elements were randomly scattered extending across the tunnel and for approximately 6 ft down the tunnel. The model fills the remainder of the tunnel up to 33 ft downstream from the entrance. The present upstream boundary conditions may not be the ideal arrangement but was selected after several days of experimentation with different upstream arrangements using roughness, vortex generators, etc. These present conditions appear to give approximate velocity profile similarity. Figure 5 shows the approach velocity and longitudinal turbulence profile for the rough upstream conditions.

In addition to the upstream modification the upper-boundary conditions (roof) was adjusted to produce a longitudinal pressure gradient along the model approximately equal to zero.

The boundary-layer development on the side walls have been measured at approximately 12 in. and with the irregular configurations of the model may affect the side flows patterns up to 18 in. Therefore, the effective width of the model which may not be affected seriously by the side wall conditions was approximately 9 ft.

3. Similitude conditions

All the experiments during this report period were conducted under neutral conditions. Therefore, according to Eq. (2.4) the concentration distribution over the model depends on a) geometric b) turbulence and c) wind velocity profile similarity viz

$$\frac{\overline{C}\,\overline{U}\,h_s^2}{Q} = f\left(\frac{Z}{H}\,,\ Re_t\,,\ U(z)/U_g\,,\ t/T\right)\,. \qquad (3.1)$$

The geometric similarity was reasonably satisfied by the topographic model. The wind velocity profile similarity was checked by utilizing wind tunnel velocity data obtained at the Pagosa Springs site on the model and wind velocity data obtained in the field at Durango. Figure 6 shows the comparison of the model wind velocity profiles for different upstream conditions and a field velocity profile.

The results with upstream roughness indicate fairly good similarity with an exception in the lower 500 meters. A number of factors which may contribute to the disparity are a) the

differences in location - Durango is more sheltered than Pagosa Springs b) difference in the lower-level wind directions in the field and c) possible insufficient roughness on the model.

Dynamic similarity was based on the concept of an aerodynamically rough flow. In this case, the freestream velocity was set at a speed high enough to insure that the airflow over the model was turbulent. Under these conditions, the form drag prevails over the viscous drag and the flow is independent of the Reynolds number. For these experiments, a freestream between 2 - 3 mps was expected to satisfy these conditions.

Nemotos criteria for a distorted model, Eq. (2.7), could not be checked because data on the eddy diffusion coefficients were not available for model or field. In the case of the San Juan model the distortion factor α is 1.4 and may be small enough that serious similarity differences may not occur. This subject will need further consideration and examination before definite statements can be made about effects of scale distortion on the modeling criteria.

4. Wind velocity and turbulence profiles

a. Procedure

The average longitudinal (streamwise) velocity $\overline{U}$, the longitudinal and lateral turbulent intensity i_x and i_y were measured by means of a yawed or rotated single hot wire mounted over the model. The wire was operated at the normal position for obtaining $\overline{U}$ and i_x and at two yawed angles 45° and 135° for i_y. Details of the theory of hot-wire measurements are too lengthy to include in this report.

Procedures followed in obtaining the measurements were similar to other studies using hot wires [Refs. 1 and 11]. Figure 7 shows a schematic diagram of the laboratory equipment for obtaining the turbulence measurements. Calibration of the hot wire (tungsten; dia ~ 0.00035 in.) was accomplished with the Thermo-System calibrator model 1125.

b. Results

Average velocity, i_x and i_y vertical profiles were obtained in 11 different locations over the model. Table 2 lists these locations along with momentum boundary-layer thickness and average lateral and longitudinal turbulent intensity values within the first ten centimeters above the model locations. The boundary-layer thickness varied from 27 to 45 cm over the model which when scaled to the field is equivalent to 15,900 ft msl to 22,750 ft msl. The depth of the boundary-layer was adequate for diffusion measurements.

A vertical cross-sectional view of selected model wind velocity profiles and turbulent intensities is shown in Fig. 8. Three of the measurement sites, Carracas Mesa, Oak Brush and Pagosa Springs are seeding generator locations.

The model wind velocities can be scaled to the field by using the following relationship:

$$\overline{U}_f = \frac{\overline{U}_m U_{g_f}}{U_{g_m}} \tag{3.2}$$

where U_{g_f} must be specified. For an example, if it was desired to estimate an average field velocity at 96 meters

from the model data at Pagosa Springs for a field freestream (geostrophic) wind of 20 m/s then from Eq. (3.2),

$$\overline{U}_f = 7 \text{ m/s}$$

when $\overline{U}_m \sim 1$ m/s , $U_{g_f} \sim 20$ m/s and $U_{g_m} \sim 2.74$ m/s .

The statistics of turbulence i_x , i_y (as well as i_z) correlate directly to the diffusing power of the model and field atmosphere. In the field, another wind fluctuation statistic often used in diffusion work is the variance, or standard deviation of the azimuthal wind-direction angle σ_θ where θ is the angular direction of the horizontal wind [Ref. 21]. This statistic is related to the intensity of turbulence in the cross-wind direction (i_y) by,

$$\sigma_\theta \sim \frac{\sigma_v}{\overline{U}} \tag{3.3}$$

According to Nemoto [Ref. 16] the model and field turbulent intensities should be matched or "similar" in neutral flow, i.e.,

$$\left.\frac{\sigma_i}{\overline{U}}\right]_m = \left.\frac{\sigma_i}{\overline{U}}\right]_f \tag{3.4}$$

In the case of the longitudinal turbulent intensities it is known from field measurements that under neutral stability conditions the variance of longitudinal velocity $(\sigma_u)^2$ is proportional to the square of the wind speed at a fixed height. Since the wind speed increases with height,

$\sigma_u/\bar{U}$ decreases upward in the boundary layer. It also seems to vary with terrain. One might expect a similar tendency in the lateral turbulent intensity [Ref. 14]. The model results as pictured in Fig. 8 suggest a similar behavior.

Estimates of the lateral and longitudinal turbulent intensity within the lower layers in mountainous terrain indicate numerical values between 10 - 25 percent and 35 percent, respectively [Refs. 18 and 22]. Model numerical values for i_x and i_y were somewhat smaller than these field estimates. This might be expected since the numerical values of i_x , i_y , i_z , σ_θ , etc., are not constants for a particular set of meteorological conditions. Their values depend on sampling and averaging times that are inherent characteristics of a sample of data. The lower model turbulence values may be due to the longer "equivalent" field sampling time required to make the measurements over the model. This inherent characteristic of the turbulence data makes it difficult for making quantitative comparisons between model and field data. The whole problem needs a thorough theoretical examination.

5. Dispersion measurements

a. Visualization of airflow and diffusion

Several experimental periods were devoted to using a chemical smoke to simulate in an approximate way the effects of the topography on a seeding plume.

The chemical used in the experiments was titanium tetrachloride ($TiCl_4$). A certain amount of the chemical was

placed in a small bottle connected to a compressed air source. When the compressed air was turned on moisture in the air reacted with the chemical and produced a visible white smoke. The chemical reaction equation is expressed as follows:

$$TiCl_4 + 2H_2O \rightarrow TiO_2 + 4HCl + \text{Heat} .$$

The white smoke is principally titanium dioxide.

The chemical smoke was released from sources on the model and photographs and movies of the smoke plume were taken over the model. A considerable amount of time was expended in experimenting with camera settings and light conditions in an attempt to find the optimum photographic conditions.

The second type of experiment consisted of placing small containers of the chemical at different source locations and letting the titanium dioxide deposit on the model surface. In these experiments a natural draft through the tunnel was used for the airstream and the wind-tunnel fan was not utilized during the course of the experiment. The freestream was between 0.5 - 1 ft/sec. Once the deposit had formed on the model, photographs and slides were taken of the patterns.

b. Radioactive gas measurements

Concentration measurements over the topographic model was obtained by releasing radioactive krypton for approximately two mins from the ground-level sources and using Geiger-Mueller tubes to determine the relative amount of krypton in samples of the gas-air mixture. The method was

originally developed by Chaudhry [Ref. 5] and was modified at a later time in order to obtain a larger number of samples at one sampling time [Ref. 6]. Figures 9 and 10 show the essential apparatus and procedure for taking samples.

Three sampling rakes of 18 probes were mounted on a traversing carriage and seven other probes were placed on the surface for collecting the gas sample released from the sources. Due to the large number of sources only two sampling positions were selected for measurements, these were a line through Wolf Creek Pass - Mt. Hope and another through Pagosa Peak - Square Top Mountain. Sampling for these two cross-sections were obtained for 15 individual sources.

In the sampling procedure, the counts of the pulses generated in the Geiger-Mueller tubes were recorded for all twenty five probes at the various locations. These counts were then transformed into concentration values using previous analysis techniques [Ref. 18]. The concentration values were determined for the known probe heights and then plotted against height.

In addition to these measurements some optimal concentration measurements were obtained downstream from Oak Brush Hill, - one of the field generator sites. The purpose of these measurements was to determine the possible terrain effects on tracer plumes released from different locations around this semi-isolated hill.

c. Results

The visualization of airflow and diffusion was not totally satisfactory due to the inherent characteristics of the chemical smoke and the problems involved with dispensing it in the wind tunnel without disturbing the ambient airstream. However, this latter problem was relatively minor once the smoke was approximately six inches from the source.

The principal results from the visualization study can be summarized as follows:

1) Meandering of the smoke plume - Smoke entering the San Juan River Valley from a source like Pagosa Springs showed a tendency to meander from the east fork to the west fork valley. Figure 11 shows a series of pictures which illustrate the meandering of the plume. This would not occur all of the time and depended on the airstream conditions as well as the configuration of the terrain.

2) Separation on the lee slopes - The separation of the airflow occurred consistently on the lee slopes of ridges. This phenomena appeared to be most dominate in the west fork valley leading up to Wolf Creek Pass.

The deposit of titanium dioxide on the model also showed the presence of separation. Figure 12 shows the chemical deposit in the east and west fork valleys of the San Juan River. The presence of the deposit on the leeward slopes of the ridges especially the west

fork valley and the minor amounts on the windward slopes were quite evident.

3) Ground deposits of titanium dioxide - Figure 13 shows the ground deposit of the chemical titanium dioxide from several simulated sources. The pattern of the deposit resembles typical ground diffusion patterns of a time-mean plume.

A selection of the results from the radioactive gas measurements is shown in Figs. 14, 15, 16, 17 and 18. Figures 14, 15 and 16 show the nondimensionalized concentration distribution at the Pagosa Peak and Wolf Creek Pass cross-section for three sources at different distances from the Wolf Creek Pass target area. The sources were chosen so as to correspond to the field generator design setup.

Figures 17 and 18 shows the concentration distribution at the Wolf Creek Pass cross-section as the result of different combinations of sources. To obtain these results it was necessary to consider the respective concentrations from each source as an additive quantity.

These results indicate that the dispersion under these stability conditions can be quite pronounced. A tentative examination of the total plume width from several of the model sources shows an average plume width of 7 miles at 7 miles from the source. Limited field data from an adjoining target area showed similar results

but with the field plume width about 1/2 mile wider than the model results.

The model results show that the vertical dispersion was very rapid. Quite often the top of the model plumes reached 20,000 ft msl. The tops of the model plumes are idealized. Effects of directional wind shear and Coriolis acceleration on the actual air motion would spread the upper region of the plumes more than was indicated in the model results.

Turning of the wind due to the Coriolis acceleration would cause the plumes to be spread more toward the east. Possible estimates of the turning effect may be made in order to correct the model results.

ELK MOUNTAIN STUDY

Contributions by

K. Kitabayashi

W. Tully

IV. ELK MOUNTAIN STUDY

Field Data

The University of Wyoming research group have provided radar-tracking data of constant-pressure balloons. These data consist of horizontal trajectories of the balloons plotted on a map of the Elk Mountain area. These trajectories have a time mark for each two minutes and height of the balloon indicated for each time mark. From these data, vertical trajectories of the balloons and streamwise velocity distributions were estimated around Elk Mountain. Figures 19 and 20 presents a selection of these data.

Generally, the constant-pressure balloon data does not show any strong divergence in the horizontal velocity field due to the presence of Elk Mountain. One possible reason was that the data were taken during strong wind conditions ($\sim$15 m/s) so that the thermal and topographic influences were not large.

Laboratory Experiments

The construction and details of the Elk Mountain model was described in earlier and Annual reports [Ref. 19]. Details of this work will not be repeated in this report.

A brief summary of the experiments accomplished in the meteorological wind tunnel for the stably-stratified airflow is presented in the following paragraphs.

The stably-stratified airflow was generated in the wind tunnel by heating the ambient air to 90°F, cooling the wind-tunnel test section floor to 30°F and also by placing 500 lbs of dry ice approximately 10 meters upwind from the topographic model. Another

purpose of the dry ice was to create an appropriate thick thermal boundary layer.

The wind-tunnel freestream velocity was approximately 20 cm/sec. Under these velocity and thermal conditions Richardson number similarity between field and model was satisfied approximately. Vertical profiles of the velocity were measured by the smoke-wire equipment. Details of this method can be found in Ref. 18.

Temperature distributions over the model were measured using fifteen thermocouples arranged vertically on a rod at 2 cm spacings. The output voltage of the thermocouples were recorded by a digital printer.

Concentration measurements over the topographic model were obtained by releasing radioactive krypton from a ground-level source located approximately 18 km (prototype scale) upstream from Elk Mountain. Samples were obtained by the same equipment as discussed in Section III.

Results

A brief summary of the results is presented in the following paragraphs. A more detailed report will be published in the near future [Ref. 10].

The vertical profiles of the horizontal velocity as determined by the smoke-wire equipment are shown in Fig. 21. These profiles were obtained from two to three photographs of the smoke-line profiles at the same location over the model. The horizontal velocity increases about 50 percent at the crest and then decreases on the lee side. The most apparent decrease in the horizontal velocity occurred just downstream from the steepest slope. This condition is analogous to the

hydraulic "jump" phenomenon. Visualization by a chemical smoke actually showed the presence of a type of hydraulic "jump".

The temperature profiles over the model are shown in Fig. 22. The model surface temperature was apparently a little higher than the air above it producing a near-neutral stability layer of approximately 8 cm ($\sim$ 800 m prototype scale) above the model surface. This type of temperature profile resembles the potential temperature vertical profile used in the University of Wyoming's computer model.

The thickness of the neutral layer was observed to decrease with the terrain elevation. The airflow characteristics of this model appear to correspond to certain aspects of the "shallow-water" theory that has been utilized to describe airflow over mountains especially on the lee side [Refs. 9 and 17].

A model Froude number was calculated based on the thickness of the neutral layer over the model. This calculation is

$$Fr = \frac{\overline{U}}{\sqrt{gh}} \sim 0.22 \qquad (4.1)$$

where $\overline{U} \sim 20$ cm/sec and $h \sim 8$ cm .

A bulk Richardson number was also calculated which is

$$Ri = \frac{g}{\overline{T}} \frac{\Delta T}{\overline{U}^2} \Delta z \sim 3.2 \qquad (4.2)$$

where $\Delta z = 20$ cm and $\overline{U} = 20$ cm/sec. This value was compared with a corresponding Richardson number in the field of

$$R_i \Big|_f \sim 1.7 \ . \qquad (4.3)$$

This latter value was calculated from the mean of ten upper air soundings near Elk Mountain.

A ground level view of the nondimensional concentration $\overline{C}\ \overline{U}\ H^2/Q$ is shown in Fig. 19. In the case H represents the height of the boundary layer which was 10 cm, $\overline{U}$ = 20 cm/sec and Q was variable depending on the distance from the source. Similar concentration data for the field were not available so the model data were compared with constant-pressure balloon trajectories that showed similar trajectory characteristics (Fig. 19).

The deflection of the tracer plume maximum concentration axis was greater for the airflow with stable conditions as compared with the neutral stability airflow results. Table 3 summarizes a number of simple calculations showing the differences in concentration patterns between the two model airflows.

In Table 3, the plume axis deflection is measured in terms of the freestream direction, the lateral plume dispersion is defined by the distance from the plume axis to the point where the concentration decreases to 60 percent of the peak value and the vertical dispersion is defined by the height where the concentration decreases to one-tenth of the ground value.

The plume-axis deflection and lateral-dispersion data show that the mountain effect was more dominate in the airflow with thermal stratification. These results were expected but unfortunately comparable field or numerical results are not available to check with the model results.

EAGLE RIVER VALLEY - CLIMAX STUDY

Contributions by

L. Hjermstad

D. Adams

D. Hill

Western Scientific Services, Inc.

V. EAGLE RIVER VALLEY - CLIMAX STUDY

Field Data

The principal objectives of the field program have been outlined previously in other reports [Ref. 19]. The main effort during this period was to obtain further data on the sampling of silver-iodide and other tracer materials by aircraft.

During the annual field program in the Climax area during the second week of December, 1970, three sampling flights were completed. These were December 11, 12 and 15. The first flight December 11 was essentially a test flight to check the instrumentation in the airplane and a test period for the ground-support people. The second and third flights on December 12 and 15 were actual data collecting flights.

The aircraft used for the sampling flights was the Aerocommander 500-B. The instrumentation consisted of the NCAR ice nucleus counter, a Mee Industries model 110 automatic fluorescent particle counter, millipore filter sampling system for ice nuclei and a simple sampling tube for collecting sulfur hexafluoride.

The particulate materials used for tracing was silver-iodide, fluorescent zinc sulfide particles and sulfur hexafluoride gas. The tracer materials were released from one site at Minturn. There was only one day, the 15th of December, when all three tracer materials were released from the source site.

The weather during December 11 and 12 was essentially clear. Obviously, these days were not typical cloud-seeding operational days. However, December 15 was typical of an operational day with considerable cloudiness and snow showers over the area. Only a selection of the

aircraft sampling data for the 12th of December will be presented in this report.

The weather for December 12 consisted of clear skies and very stable atmospheric stability conditions within the Eagle River Valley (Fig. 23). Surface winds in the valley were light and variable but were northwest and stronger at the Leadville airport. A constant-volume balloon launched from Minturn in the early afternoon showed that the average winds above the ridge tops were west-northwest between 16 or 17 mps (Fig. 24).

The Minturn generator was turned on at 0700 hrs and continued until 1800 hrs. The aircraft sampling started at 14:13 MST and ended at 15:53 MST. The aircraft sampling was delayed until the afternoon due to poor dispersive wind conditions in the morning.

The distribution of silver-iodide concentration with respect to the terrain for three sampling passes in the area is depicted in Fig. 25. The altitude of these flights varied from 11,500 ft to 13,000 ft msl. The horizontal trajectories of these three passes are shown in Fig. 24.

The concentration values have been increased by a factor of ten since the present NCAR Ice Nucleus counter underestimates the actual nuclei count because of an altitude induced error [Ref. 12]. An average count of ice nuclei (at -21°C) at different places during the sampling was obtained by the millipore filter sampler, are shown in Fig. 25 as horizontal lines with the average concentration above the line.

The NCAR Ice Nucleus counter data was averaged over the same time periods in which filter data were taken and then compared to the

respective filter data. For counts over 200 nuclei/liter the NCAR counter data were approximately 50 percent higher than the filter data. For lower counts the differences were on the order of 10 percent.

The dispersion of the silver-iodide plume resembled that of other days in that the highest counts were observed within the valley. The vertical dispersion was larger than expected for a day with light lower-level winds and stable stability. A few counts above 10 nuclei/liter were detected at 13,000 ft msl approximately 20 - 25 km from the Minturn source. If the 10 nuclei/liter value is taken as the boundary of the plume, a rough estimate may be made on the horizontal dispersion. At 10 km from the source the plume was on the order of 6 km in width. At 20 km, the plume width broadens considerably probably exceeding 16 km in width. A 30 km, the plume was diluted so much that a plume boundary was difficult to estimate from the limited measurements.

The tentative concensus from these results is that during long duration seeding from ground generators the seeding material can be significantly dispersed in the vertical and lateral directions under stable stability conditions. Although the physical mechanisms for dispersing the seeding material are not readily apparent in these measurements our previous measurements with dual constant-volume balloons suggest orographically induced eddies as one reasonable explanation for the significant dispersion.

Laboratory Experiments

All the experimental work has been completed on this model and the results have been reported in a technical report [Ref. 18].

VI. FUTURE WORK

The principal effort for the next few months will be directed toward finishing laboratory experiments with the San Juan model. Some additional experiments and photography with thermal stratification will take up the remaining time.

Experiments with the Elk Mountain and the Eagle River Valley model are essentially finished. No further experiments are planned.

ACKNOWLEDGMENTS

Dr. R. Dirks and others of the University of Wyoming have assisted us by providing field data for Elk Mountain. Western Scientific Services, Inc., of Fort Collins and EG & G of Durango have assisted by providing information and data for the Wolf Creek Pass - Pagosa Springs area.

Mee Industries, Inc., and Dr. G. Langer of the National Center of Atmospheric Research assisted the project by providing sampling equipment.

REFERENCES

1. Arya, S.P.S., 1968: Structure of stably stratified turbulent boundary layer. Ph.D. dissertation, College of Engineering, Colorado State University.

2. Bergeron, T., 1949: The problem of artificial control of rainfall on the globe. Tellus 1, 32-50.

3. Cermak, J.E., and Arya, S.P.S., 1970: Problems of atmospheric shear flows and their laboratory simulation. Boundary-Layer Meteorology 1, 40-60.

4. Chappell, C.F., Grant, L.O. and Mielke, P.W., 1969: Operational definition for weather modification applications to orographic clouds. Internal Report, Colorado State University, Department of Atmospheric Science.

5. Chaudhry, F.H., 1969: Turbulent diffusion in a stably stratified shear layer. Ph.D. dissertation, College of Engineering, Colorado State University.

6. Chaudhry, F.H. and Cermak, J.E., 1971: Simulation of flow and diffusion over an urban complex. Technical Report ECOM-0423-7; CER70-71FHC-JEC24, Fluid Dynamics and Diffusion Laboratory, Colorado State University.

7. EG & G, 1970: Installation and operation of an opportunity recognition and cloud seeding system for operational weather modification research in Colorado. Phase I Comprehensive Field Report. Bureau of Reclamation Contract No. 14-06-0-6963, Boulder, Colorado.

8. Grant, L. O. et al., 1969: An operational adaptation program of weather modification for the Colorado River Basin. Interim Report, Department of Atmoshperic Science, Colorado State University.

9. Houghton, D.D. and Kasahara, A., 1968: Nonlinear shallow fluid flow over an isolated ridge. Communications on Pure and Applied Mathematics, Vol. 21, 1-23.

10. Kitabayashi, K., Orgill, M.M. and Cermak, J.E., 1971: Laboratory simulation of airflow and atmospheric transport-dispersion over Elk Mountain, Wyoming. Technical Report CER70-71KK-MMO-JEC-65, Fluid Dynamics and Diffusion Laboratory, Colorado State University.

11. Kung, R.L. and Plate, E.L., 1970: Boundary layer development over equally spaced fences. Technical Report CER69-70RLK-ELP-33. Fluid Dynamics and Diffusion Laboratory, Colorado State University.

REFERENCES - (Continued)

12. Langer, G., 1969: Evaluation of NCAR ice and cloud condensation nucleus counters. Proceedings of 7th International Conference on Condensation and Ice Nuclei, Prague and Vienna, Czechoslovakia, 288-292.

13. Ludlam, F.H., 1955: Artificial snowfall from mountain clouds. Tellus, Vol. 7, 277-290.

14. Lumley, J.L. and Panofsky, H.A., 1964: The structure of atmospheric turbulence. Interscience Publishers, New York.

15. McVehil, G.E., Ludwig, G.R. and Sundaram, T.R., 1967: On the feasibility of modeling small scale atmospheric motions. CAL Report No. ZB-2328-P-1. Cornell Aeronautical Laboratory.

16. Nemoto, S., 1961: Similarity between natural wind in the atmosphere and model wind in a wind tunnel - Modeling criteria for a local wind. Papers in Meteorology and Geophysics, Vol. 12, No. 1, 30-52.

17. Oobayashi, T., 1970: A numerical study of two-dimensional airflow over an isolated mountain. Journal of the Meteorological Society of Japan, Vol. 48, No. 2, 118-128.

18. Orgill, M.M., 1971: Laboratory simulation and field estimates of atmospheric transport-dispersion over mountainous terrain. Ph.D. dissertation, Department of Civil Engineering, Colorado State University.

19. Orgill, M.M., Cermak, J.E. and Grant, L.O., 1970: Research and development technique for estimating airflow and diffusion parameters in connection with the atmospheric water resources program. Annual Report CER70-71MMO-JEC-LOG-23, Fluid Dynamics and Diffusion Laboratory, Colorado State University.

20. Sutton, O.G., 1953: Micrometeorology. McGraw-Hill, New York.

21. U.S. Atomic Energy Commission, 1968: Meteorology and Atomic Energy. USAEC Division of Technical Information, Oak Ridge, Tennessee.

22. Wooldridge, G., 1970: Personal communication.

APPENDIX I

APPENDIX I

SIMILITUDE PARAMETERS

Rossby No. -- $Ro = \frac{U^*}{fL^*}$ -- Non-dimensional ratio of the inertial force to the coriolis force.

Reynolds No. -- $Re = \frac{U^*}{L^* \nu}$ or $\frac{U^*}{L^* K_m}$ -- Non-dimensional ratio of the inertial force to the viscous force.

Richardson No. -- $Ri = g \frac{1}{\Theta} \frac{\partial\Theta/\partial Z}{(\partial U/\partial Z)^2}$ -- Non-dimensional number arising in the study of shearing flows of a stratified fluid. Number expresses a characteristic ratio of work done against gravitational stability to energy transferred from mean to turbulent motion.

Prandtl No. -- $Pr = \frac{c_p \mu}{k}$ -- Non-dimensional ratio between the product of heat advection and viscous forces and the product of heat diffusion and inertia forces.

Euler No. -- $Eu = \frac{\Delta P}{\rho U^{*2}}$ -- Non-dimensional ratio between the pressure force and the inertia force.

Péclet No. -- $Pe = \frac{U^* L^*}{\kappa}$ -- Non-dimensional ratio between inertial force and mass diffusivity.

TABLES

TABLE 1

EG and G PROJECT GENERATOR SITES FOR THE SAN JUAN MOUNTAIN AREA

1. Parmley Ranch
2. Fort Lewis
3. Stocker Ranch
4. Royce Ranch
5. Sutton Ranch
6. Halliburton Ranch
7. Generator Site - Remote
8. Herrboldt Ranch
9. Ignacio Site
10. Moore Ranch
11. Sisk Ranch
12. A.T. and T. Microwave - Remote
13. Halverson Ranch
*14. Devil Mountain - Remote
15. Cooper Ranch - Remote
16. Baldamar Ranch
17. Radcliff Ranch
18. Espinosa Ranch
19. Carracas Mesa - Remote
20. American Mesa - Remote
21. Hott Ranch
22. Harris Ranch
23. Oak Brush - Remote
24. King Ranch
25. Formwalt Ranch
26. Hudson Ranch
27. Eightmile Mesa - Remote
28. Archuleta Mesa Remote
29. Wirt Lookout - Remote
30. Blue Mountain - Remote
31. V-Mountain - Remote
32. Abeyta Mesa - Remote
33. Crowley Ranch

*Generator sites underlined were constructed on the topographic model. In addition, eight other sites were constructed for optional measurements.

TABLE 2

MOMENTUM BOUNDARY LAYER THICKNESS AND AVERAGE LATERAL AND LONGITUDINAL TURBULENT INTENSITIES OVER THE SAN JUAN TOPOGRAPHIC MODEL

Location	Meters & Feet Elevation	Boundary Layer Thickness Model (cm)	Boundary Layer Thickness ft and m Prototype	Boundary Layer Thickness ft and m Prototype (msl)	Average Longitudinal (%) Turbulence Z=10 cm (960m)	Average Lateral (%) Turbulence Z=10 cm (960m)
Carracas Mesa	7,400 ft 2,256 m	27	8,502 2,592	15,902 4,848	12.0	8.3
Oak Brush Hill	8,500 ft 2,591 m	30	9,446 2,880	17,946 5,471	14.4	10.7
Chris Mountain	8,000 ft 2,439 m	30	9,446 2,880	17,446 5,319	16.1	9.1
Pagosa Springs	7,100 ft 2,165 m	40	12,595 3,840	19,695 6,005	17.6	12.4
Blue Mountain	8,870 ft 2,704 m	40	12,595 3,840	21,465 6,544	14.4	9.0
San Juan River Junc.	7,660 ft 2,335 m	45	14,169 4,320	21,829 6,655	10.6	8.0
Pagosa Peak	12,640 ft 3,854 m	25	7,872 2,400	20,512 6,254	11.4	6.8
Square Top Mountain	11,760 ft 3,585 m	30	9,446 2,880	21,206 6,465	9.6	6.7
Wolf Creek Pass	10,675 ft 3,255 m	30	9,446 2,880	20,121 6,135	20.6	6.2
Mountain Hope	12,834 ft 3,913 m	27	8,502 2,592	21,336 6,505	21.3	10.6
Summit Peak	13,300 ft 4,055 m	30	9,446 2,880	22,746 6,935	15.8	8.7

TABLE 3

ELK MOUNTAIN STUDY
PLUME AXIS DEFLECTION FROM FREE STREAM DIRECTION

X km	Neutral			Stable		
	Plume Axis Deflection km	Lateral Dispersion km	Vertical Dispersion km	Plume Axis Deflection km	Lateral Dispersion km	Vertical Dispersion km
5	0	0.46	0.57	----	----	----
10	<0.1	0.68	0.95	1.2	0.55	0.77
15	0.35	0.97	1.2	1.5	0.87	1.15
20	1.2	1.15	2.1	1.5	1.85	0.78

Lateral plume dispersion was defined by the distance from the plume axis to the point where the concentration decreases to 60 percent of the peak value.

Vertical dispersion was defined by the height where the concentration decreases to one-tenth of the ground value.

FIGURES

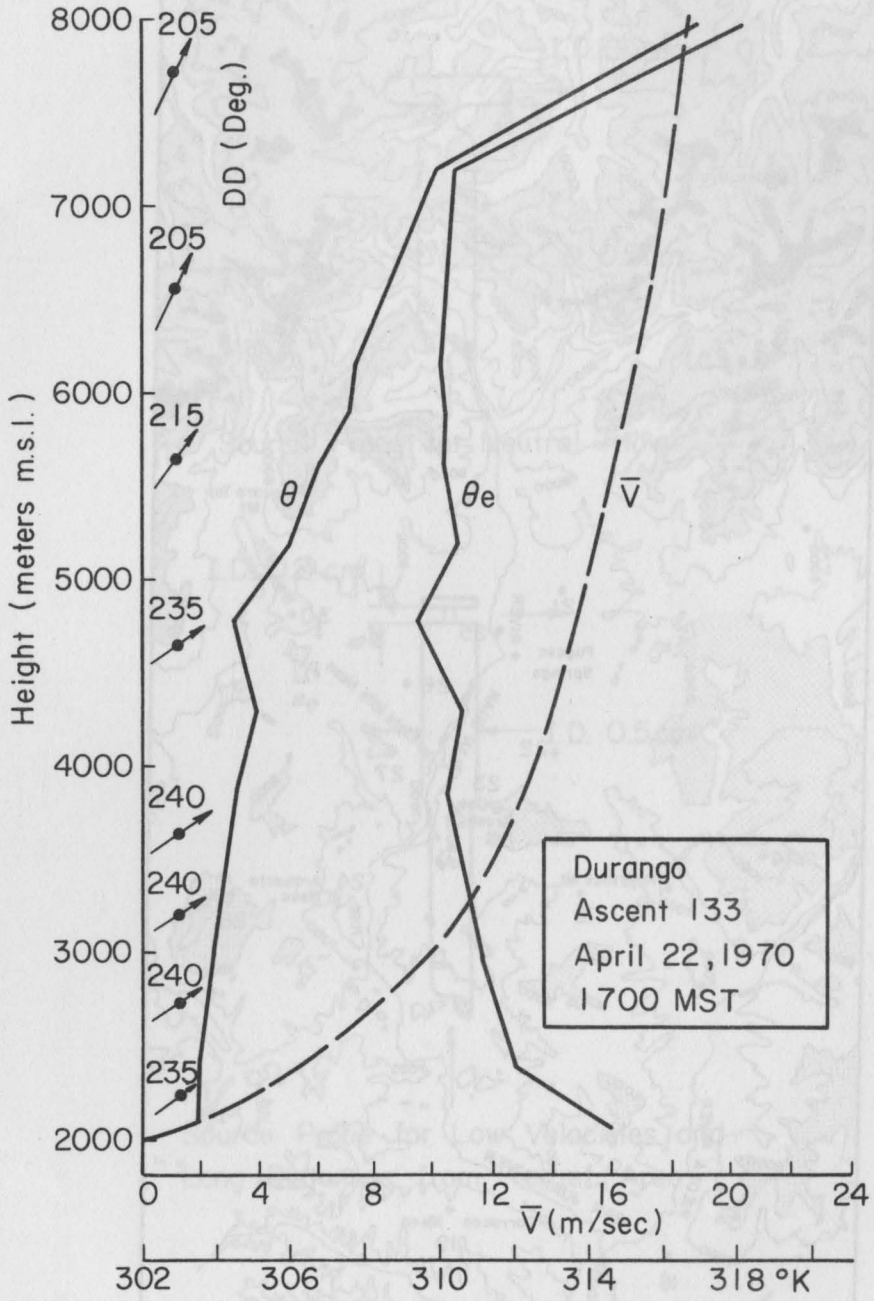

Fig. 1. Potential and equivalent potential temperature and horizontal wind distribution with height at Durango, Colorado. April 22, 1970.

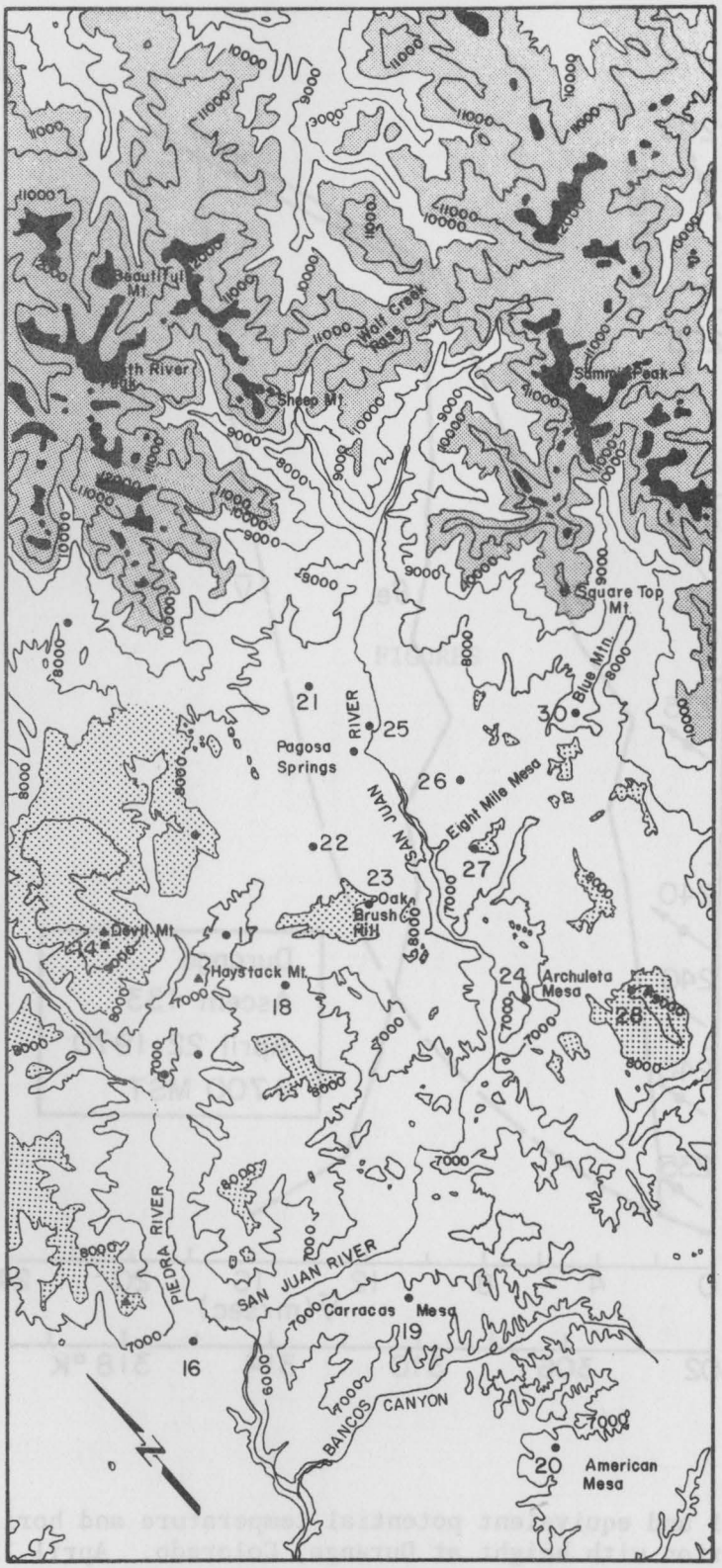

Fig. 2. Location of field generator sites that were modeled for the San Juan topographic model (see Table 1).

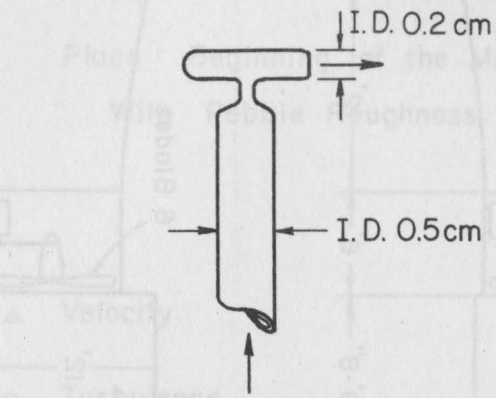

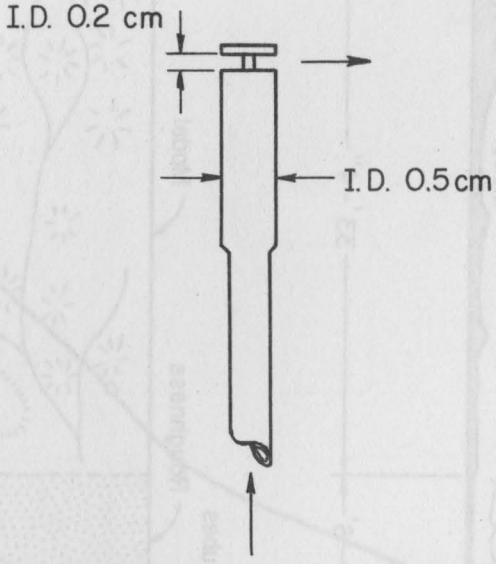

Fig. 3. Types of sources designed and utilized on the model for emitting radioactive gas.

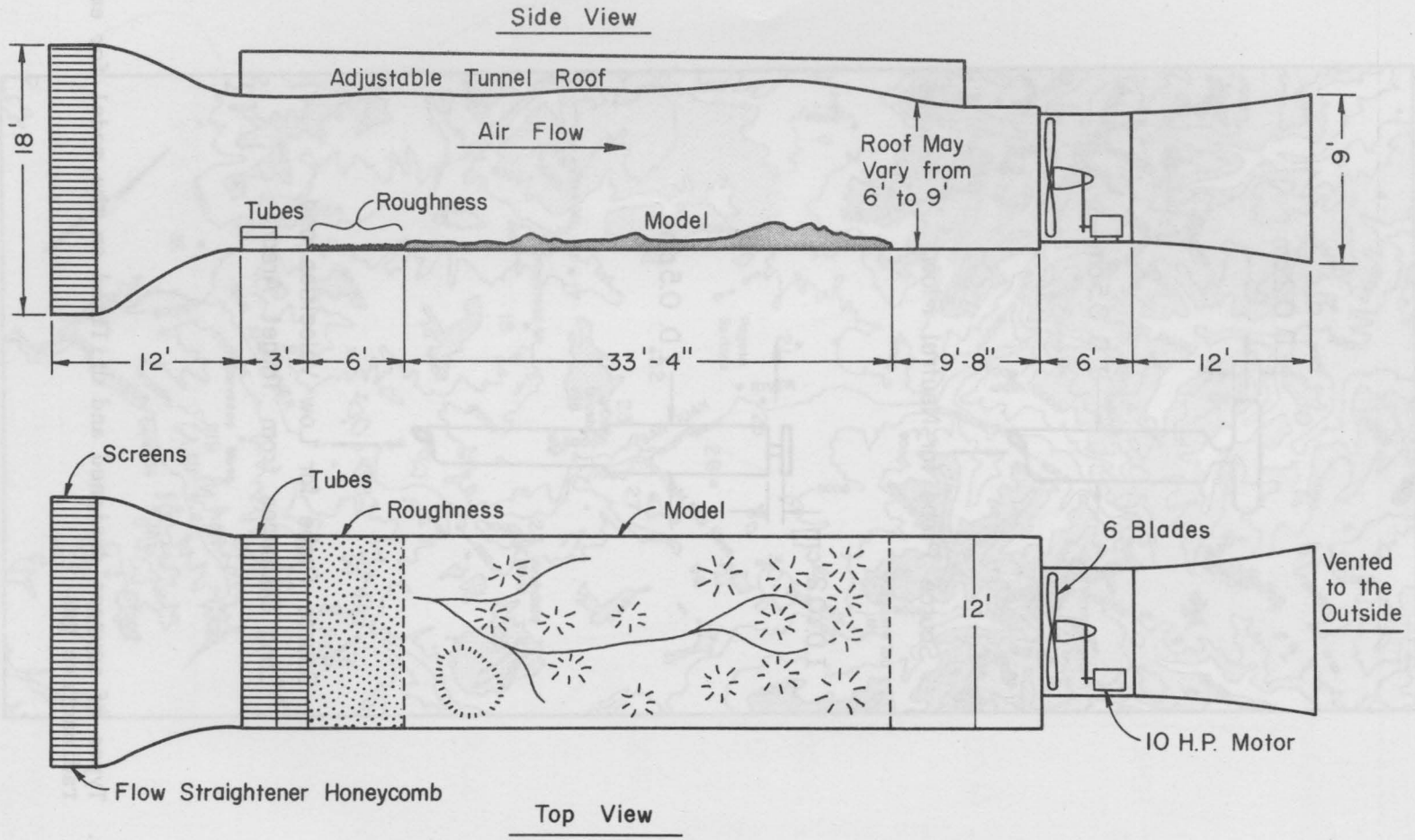

Fig. 4. Schematic diagrams of the Colorado State University environmental wind tunnel and upstream boundary conditions.

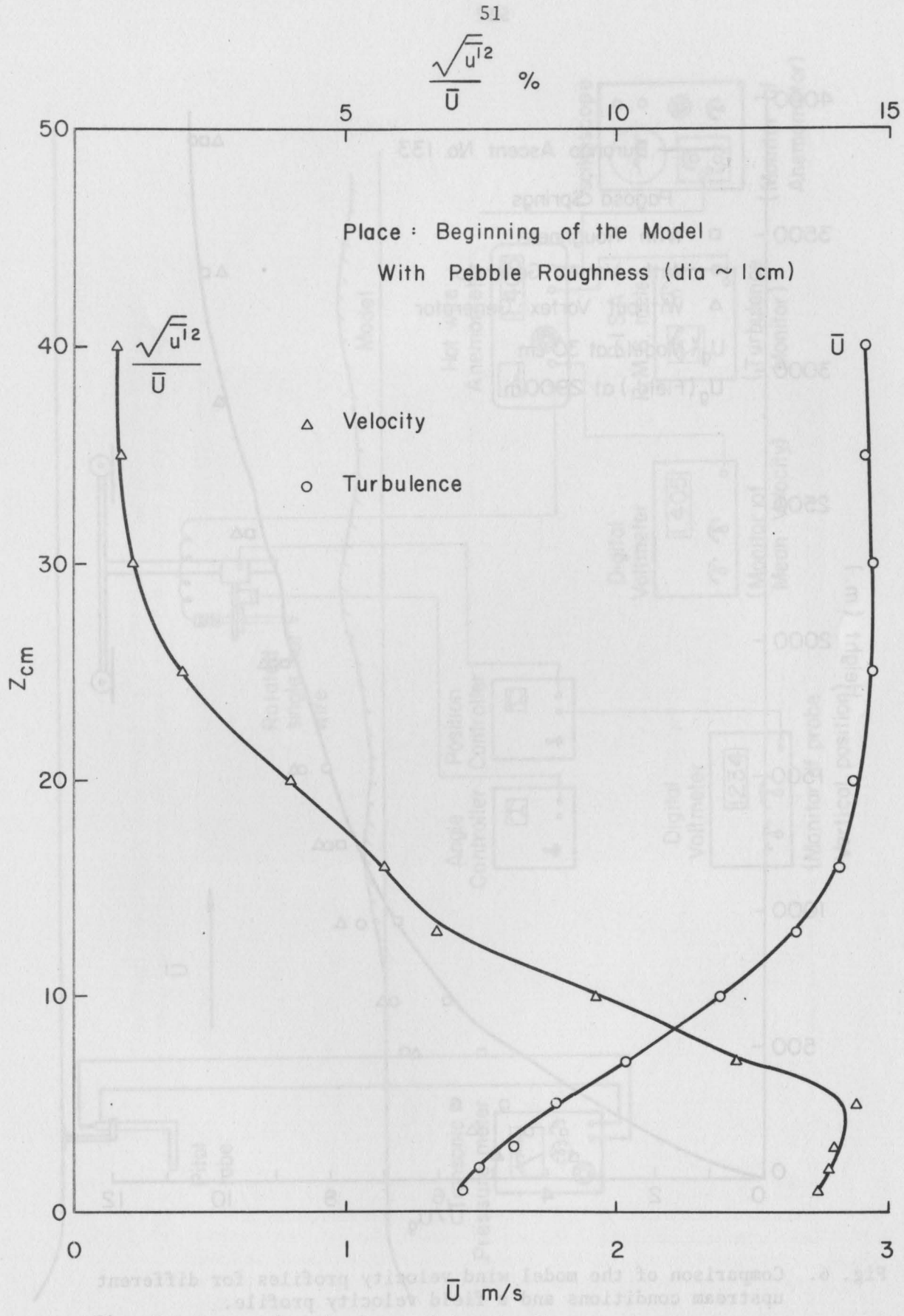

Fig. 5. Approach velocity and longitudinal turbulence profiles for the roughness upstream conditions. Scale ratio: 1 cm ≡ 96 m .

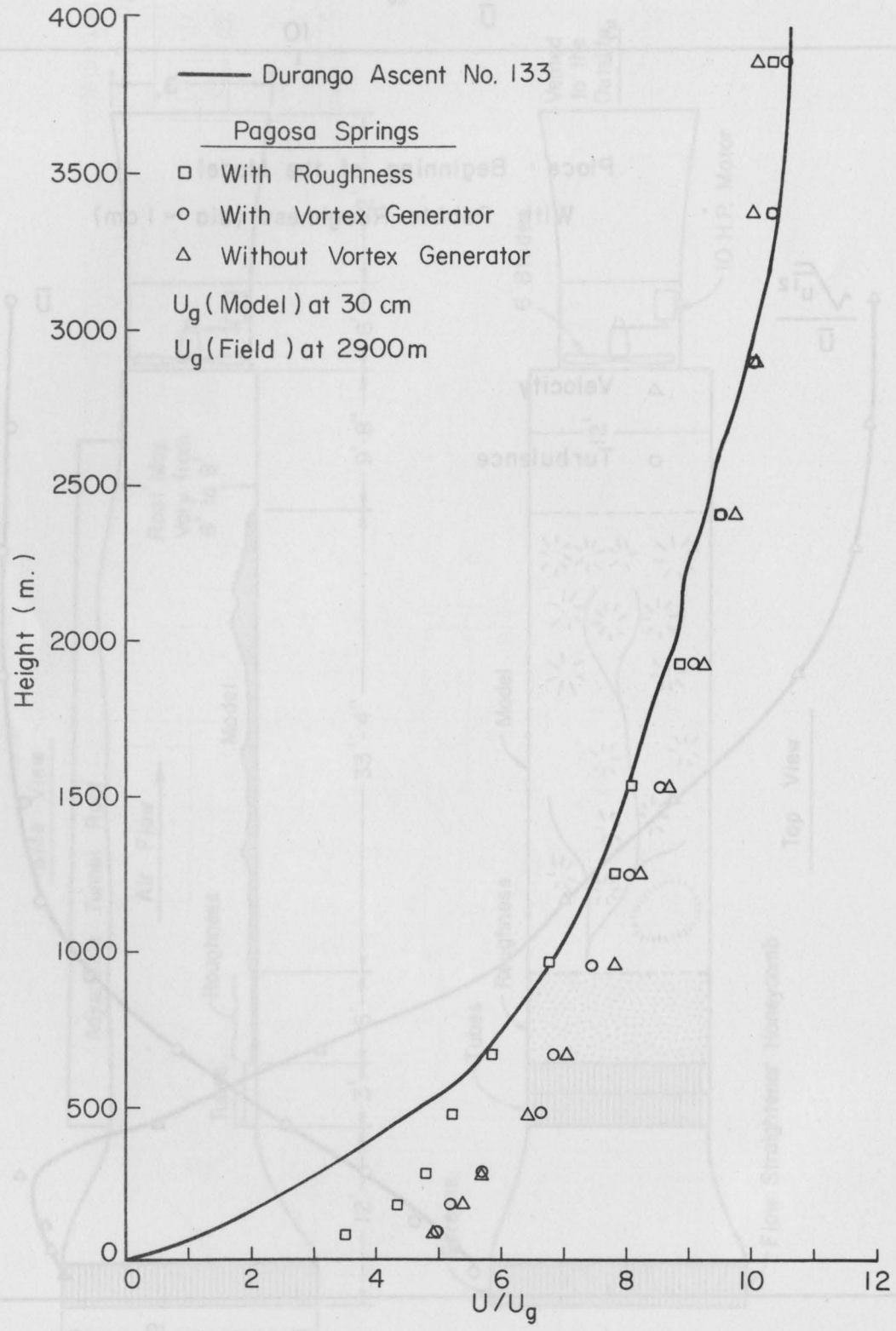

Fig. 6. Comparison of the model wind velocity profiles for different upstream conditions and a field velocity profile.

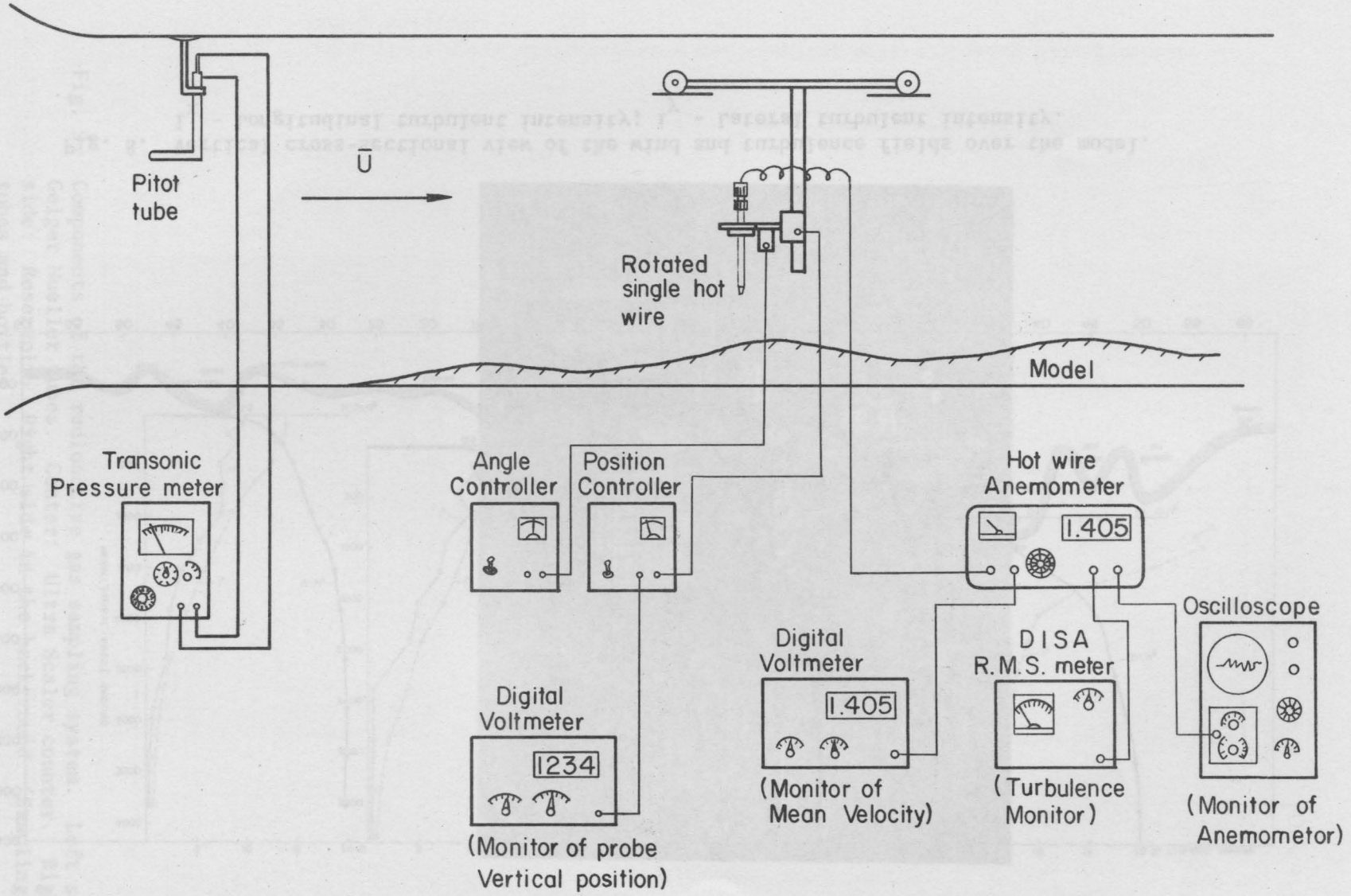

Fig. 7. Schematic diagram of the laboratory equipment for obtaining average longitudinal velocities, longitudinal and lateral turbulent intensities.

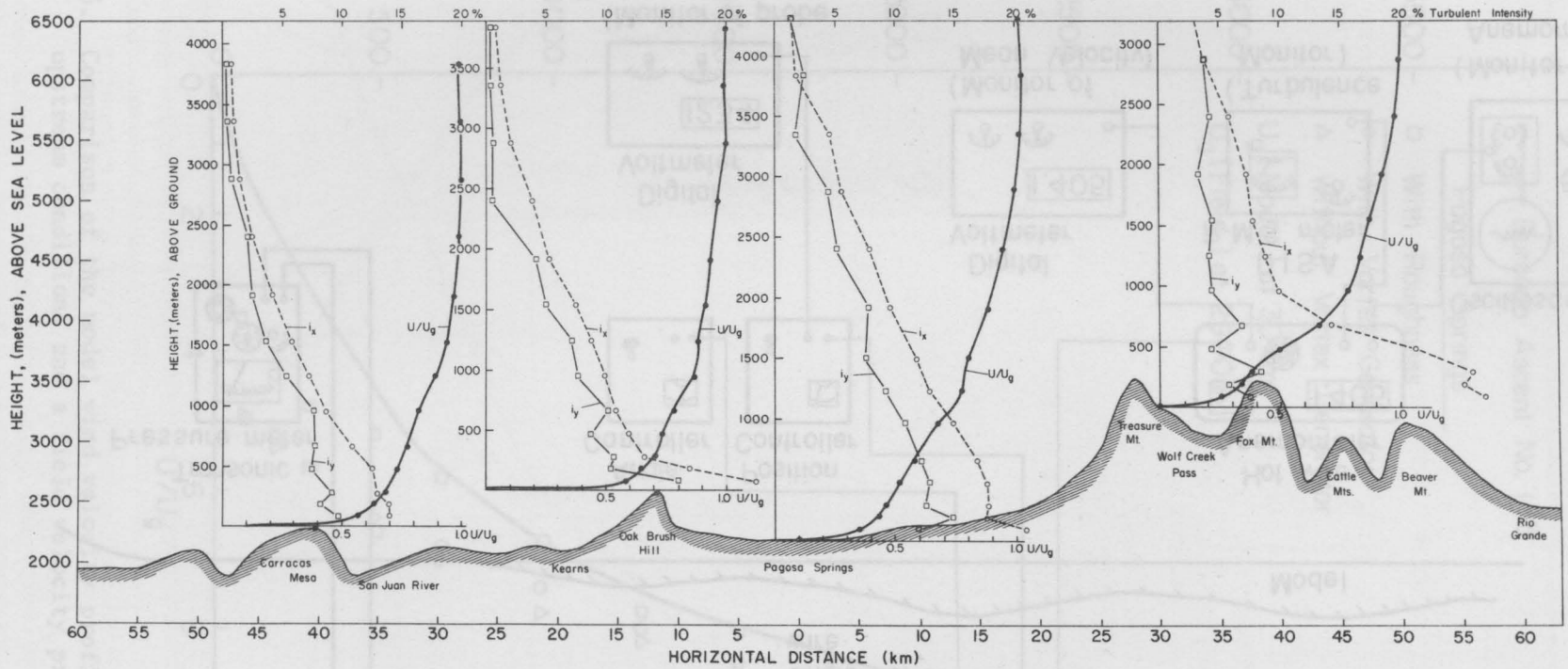

Fig. 8. Vertical cross-sectional view of the wind and turbulence fields over the model. i_x - Longitudinal turbulent intensity; i_y - Lateral turbulent intensity.

Fig. 9. Components of the radioactive gas sampling system. Left side: Geiger Mueller tubes. Center: Ultra Scaler counter. Right side: Reservoir. Right side in the background: Sampling tubes and bottles.

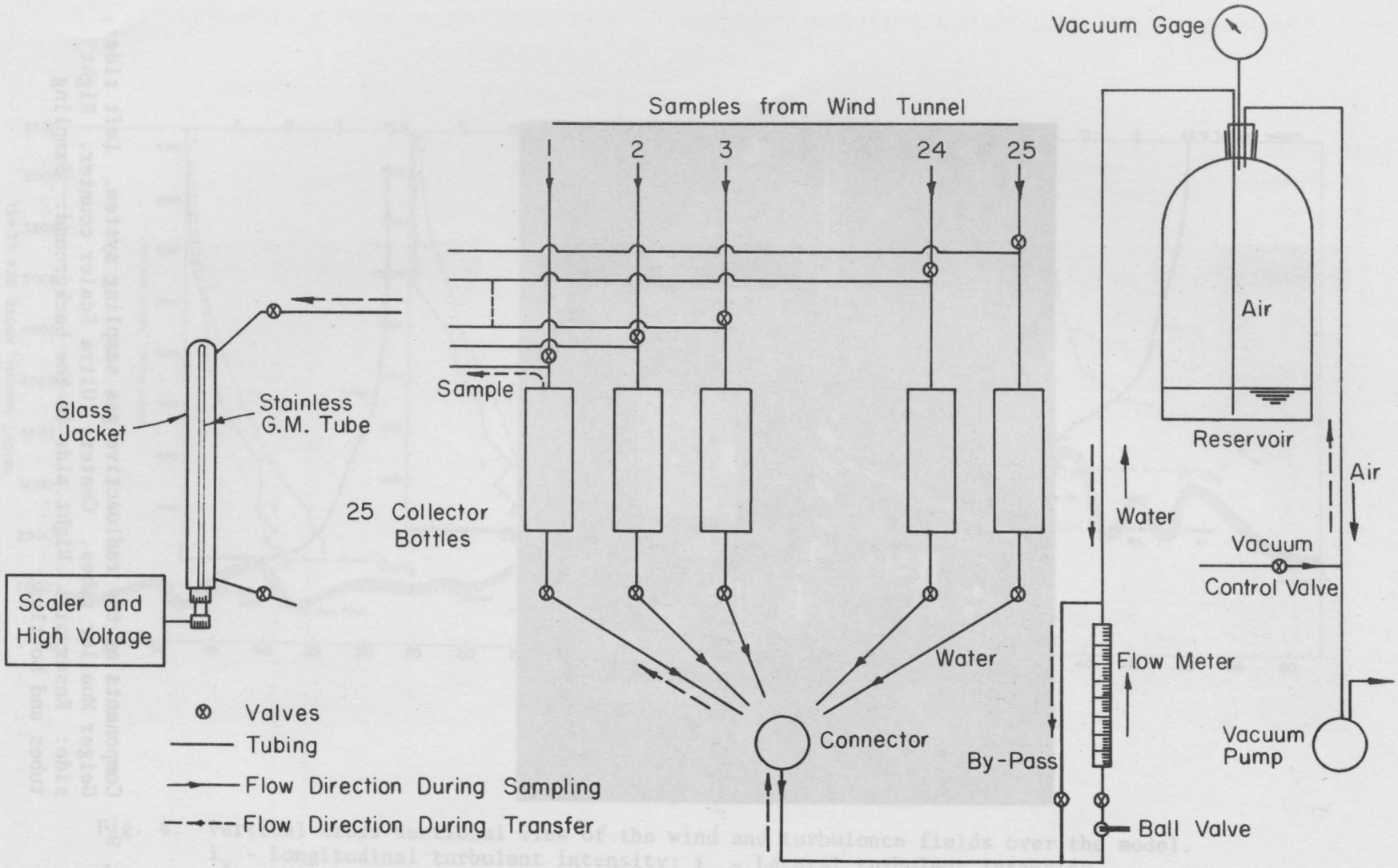

Fig. 10. Schematic diagram of radioactive gas sampling system showing flow direction during sampling.

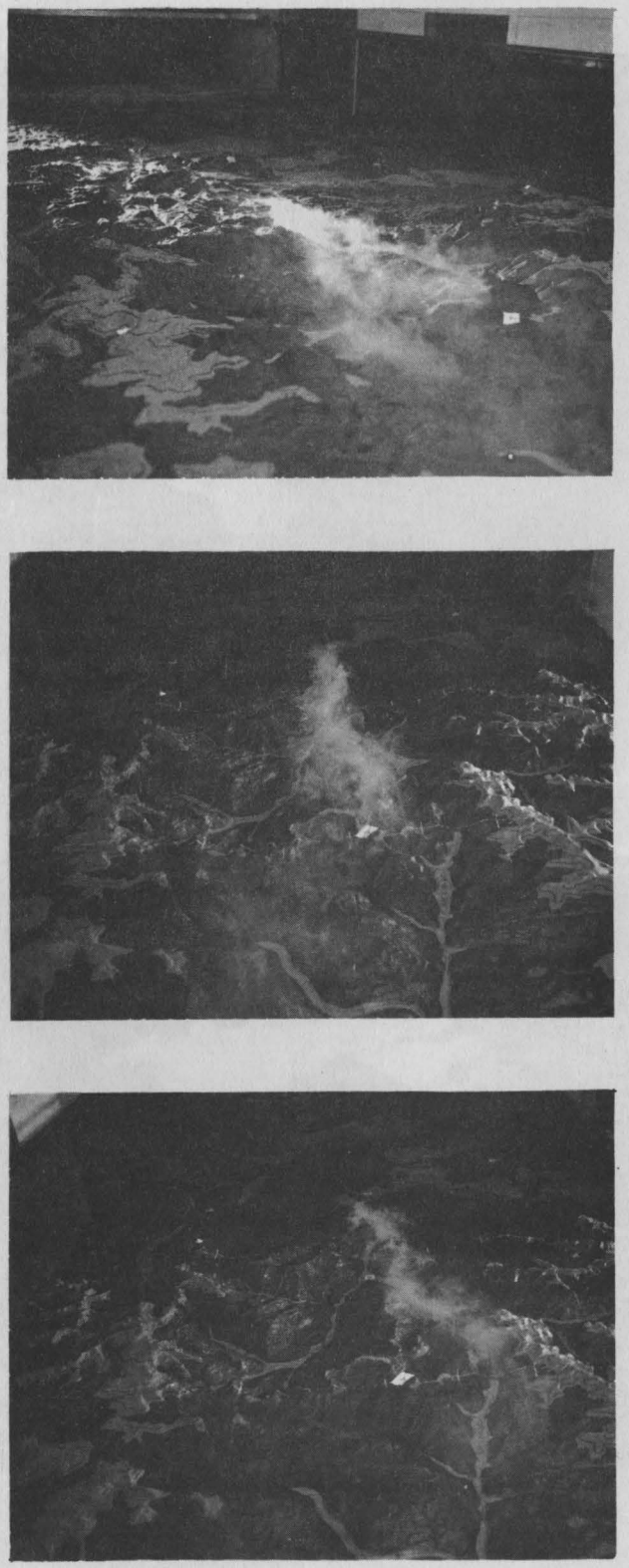

Fig. 11. Pictures illustrating meandering of the smoke plume with time in the wind tunnel. White patch in foreground is Wolf Creek Pass. Pagosa Springs source.

Looking downstream

Looking upstream

Fig. 12. Titanium dioxide deposit in the east and west fork valleys of the San Juan river illustrating the effects of separation of the airflow.

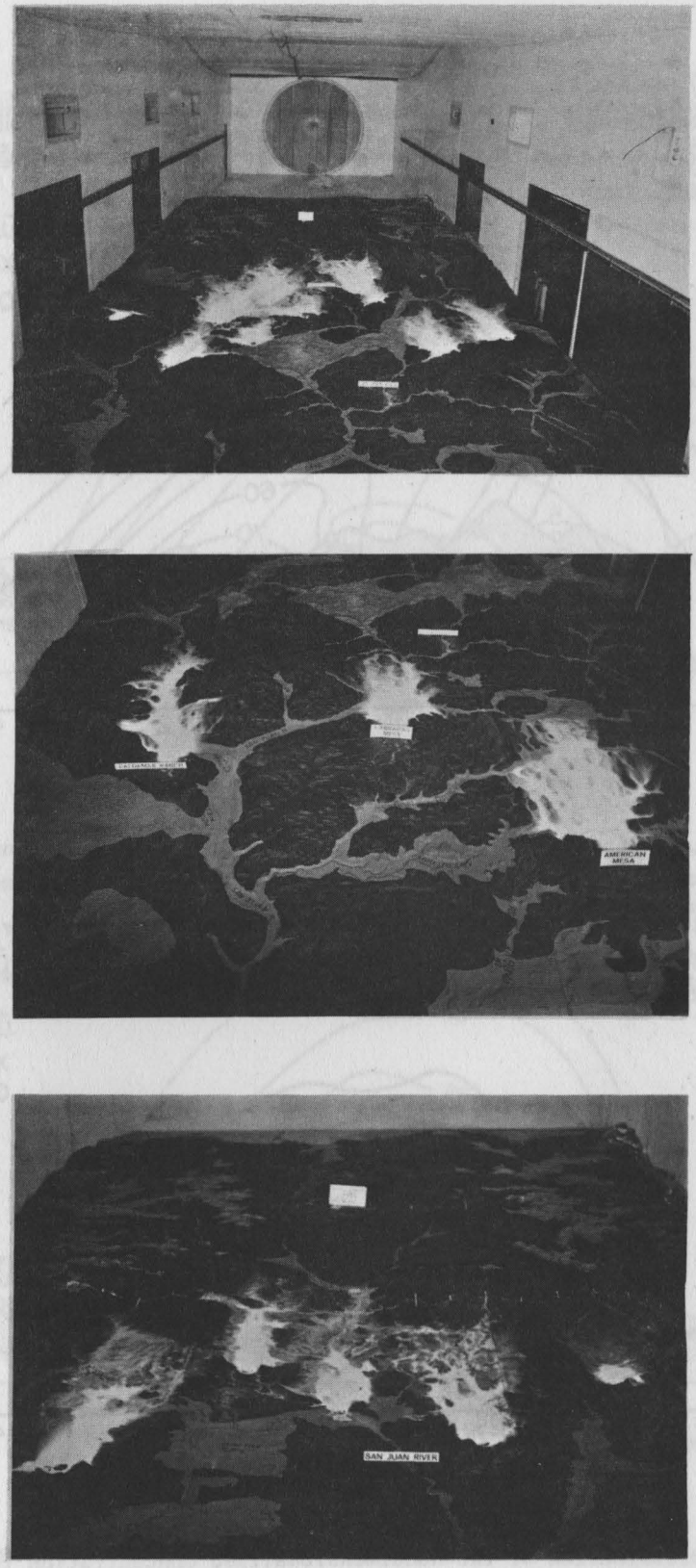

Fig. 13. Ground deposit as the result of chemical smoke from different simulated sources. Looking downstream.

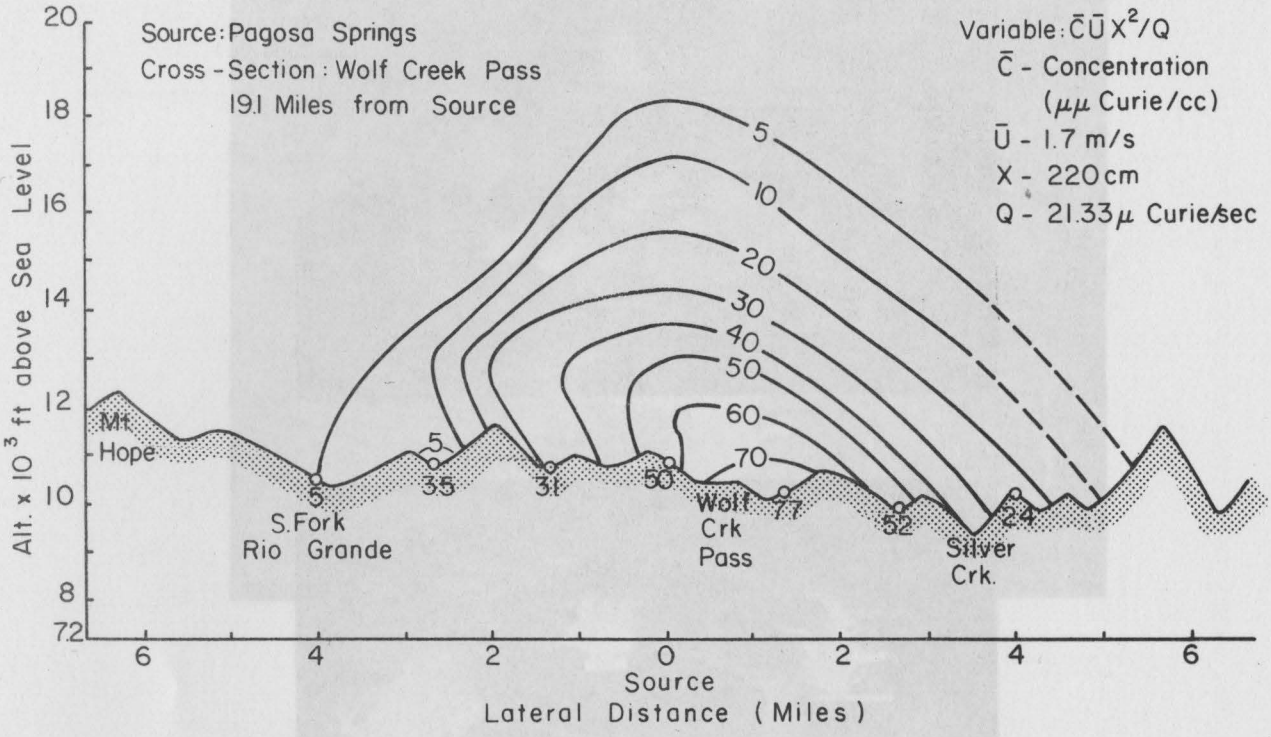

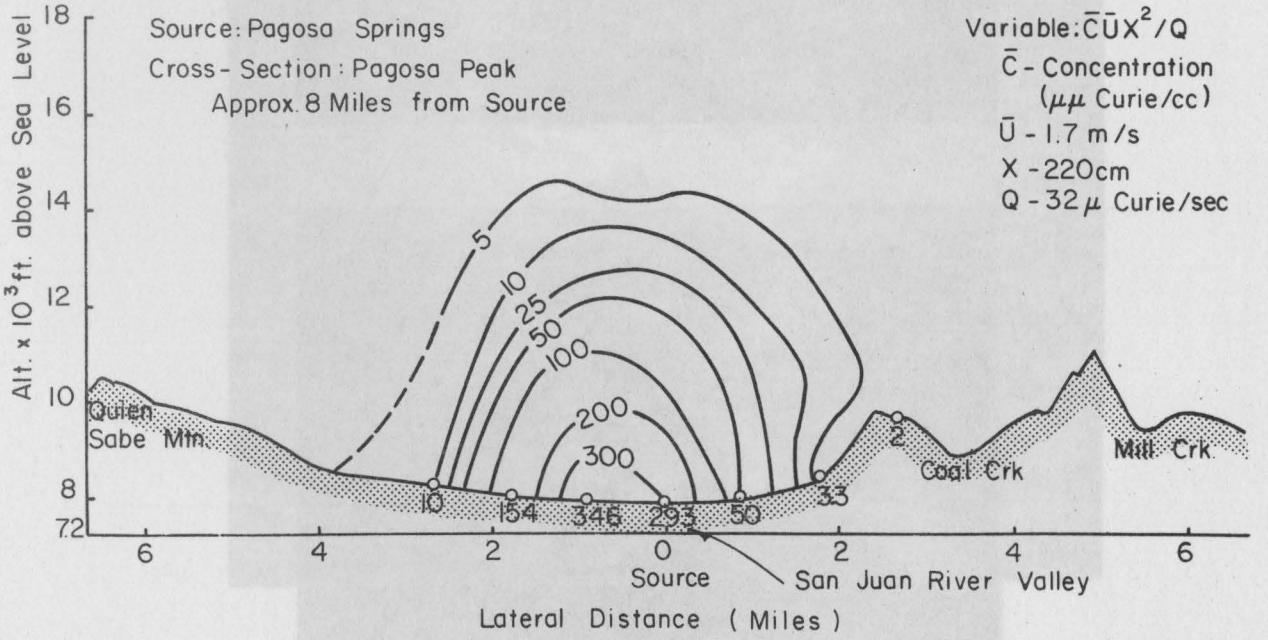

Fig. 14. Distribution of the nondimensionalized concentration for two lateral cross-sections over the model. Source: Pagosa Springs. X - Model distance from Wolf Creek Pass to Pagosa Springs.

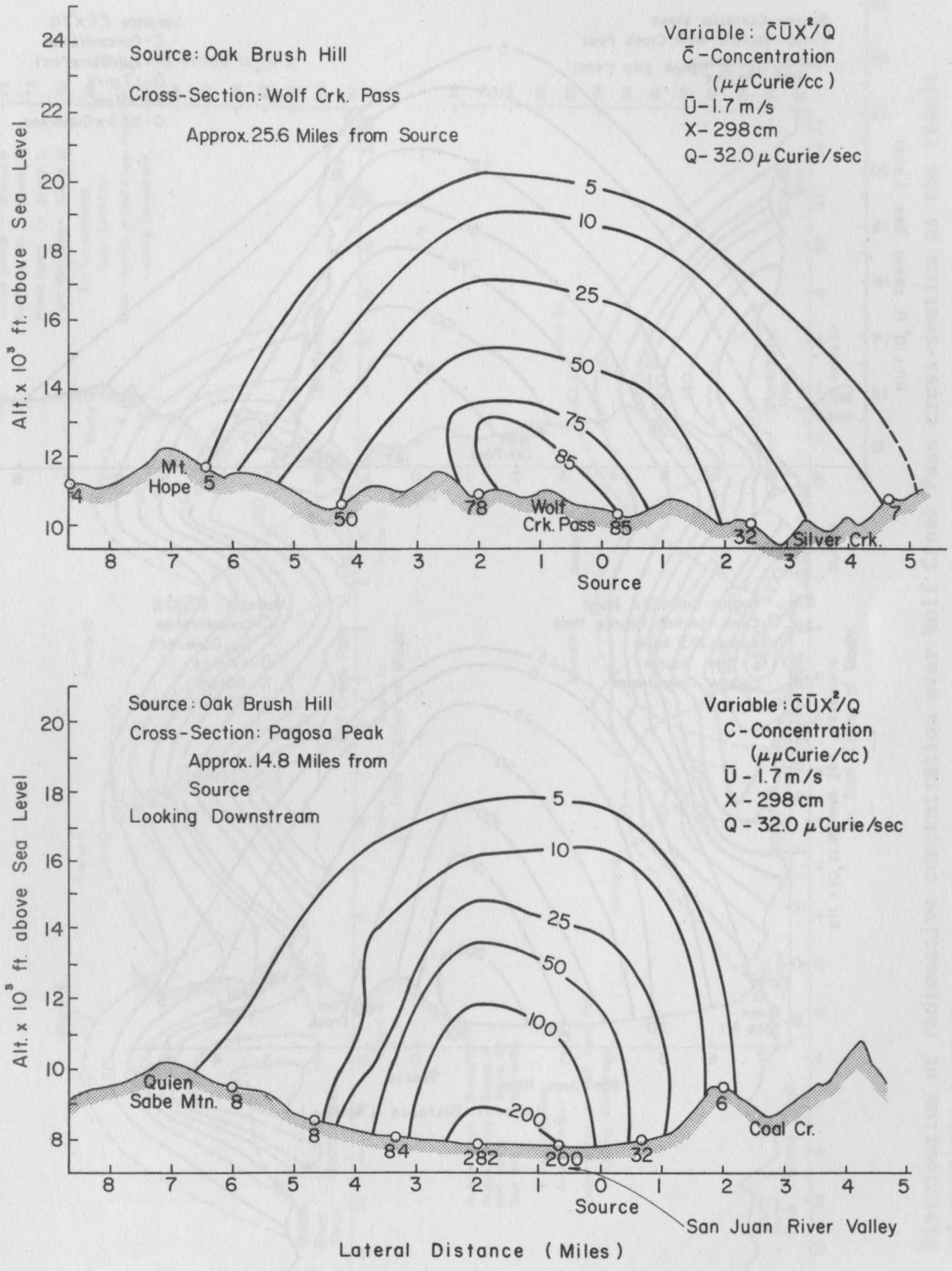

Fig. 15. Distribution of the nondimensionalized concentration for two lateral cross-sections over the model. Source: Oak Brush Hill. X - Model distance from Oak Brush Hill to Wolf Creek Pass.

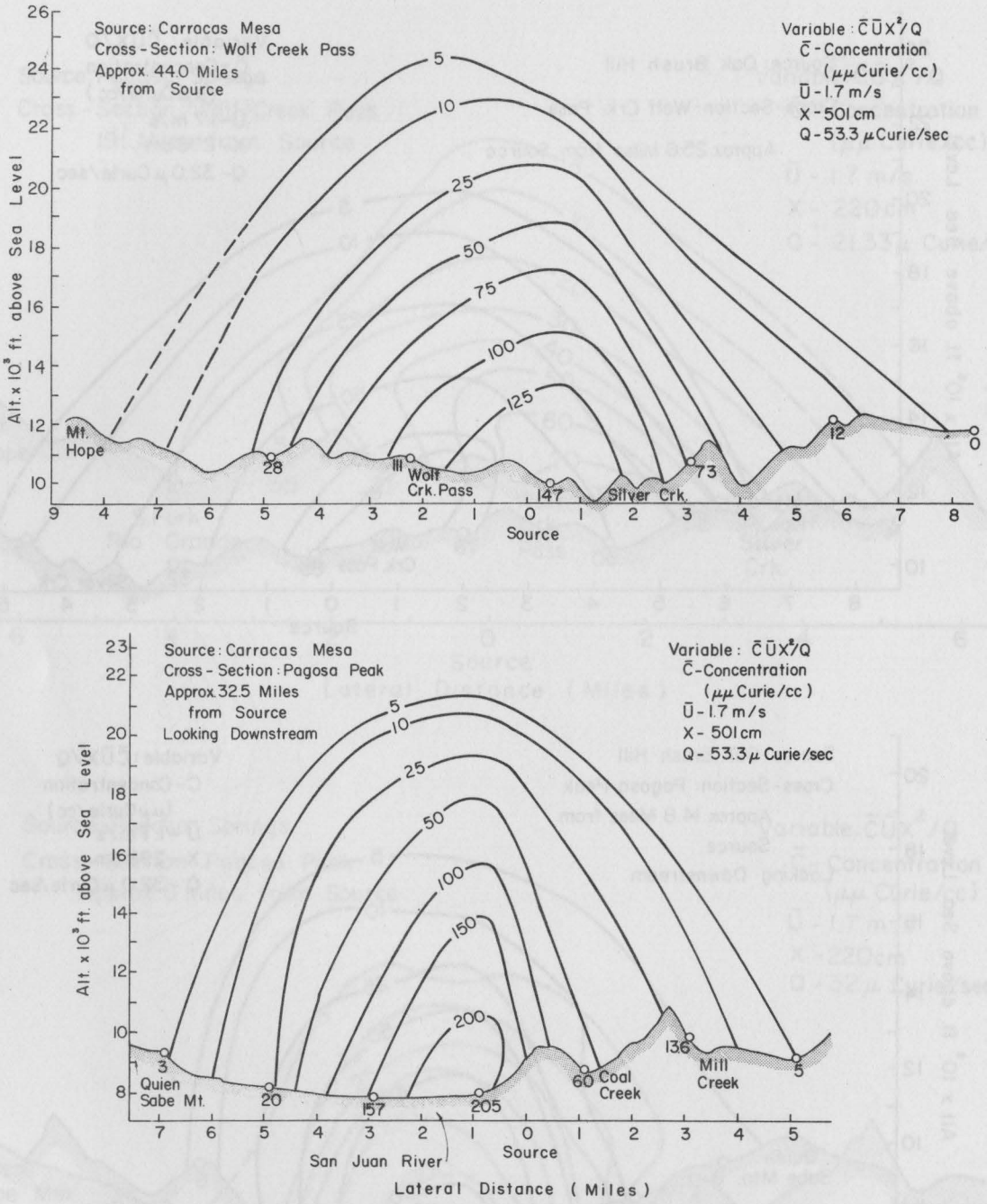

Fig. 16. Distribution of the nondimensionalized concentration for two lateral cross-sections over the model. Source: Carracas Mesa. X - Model distance from Carracas Mesa to Wolf Creek Pass.

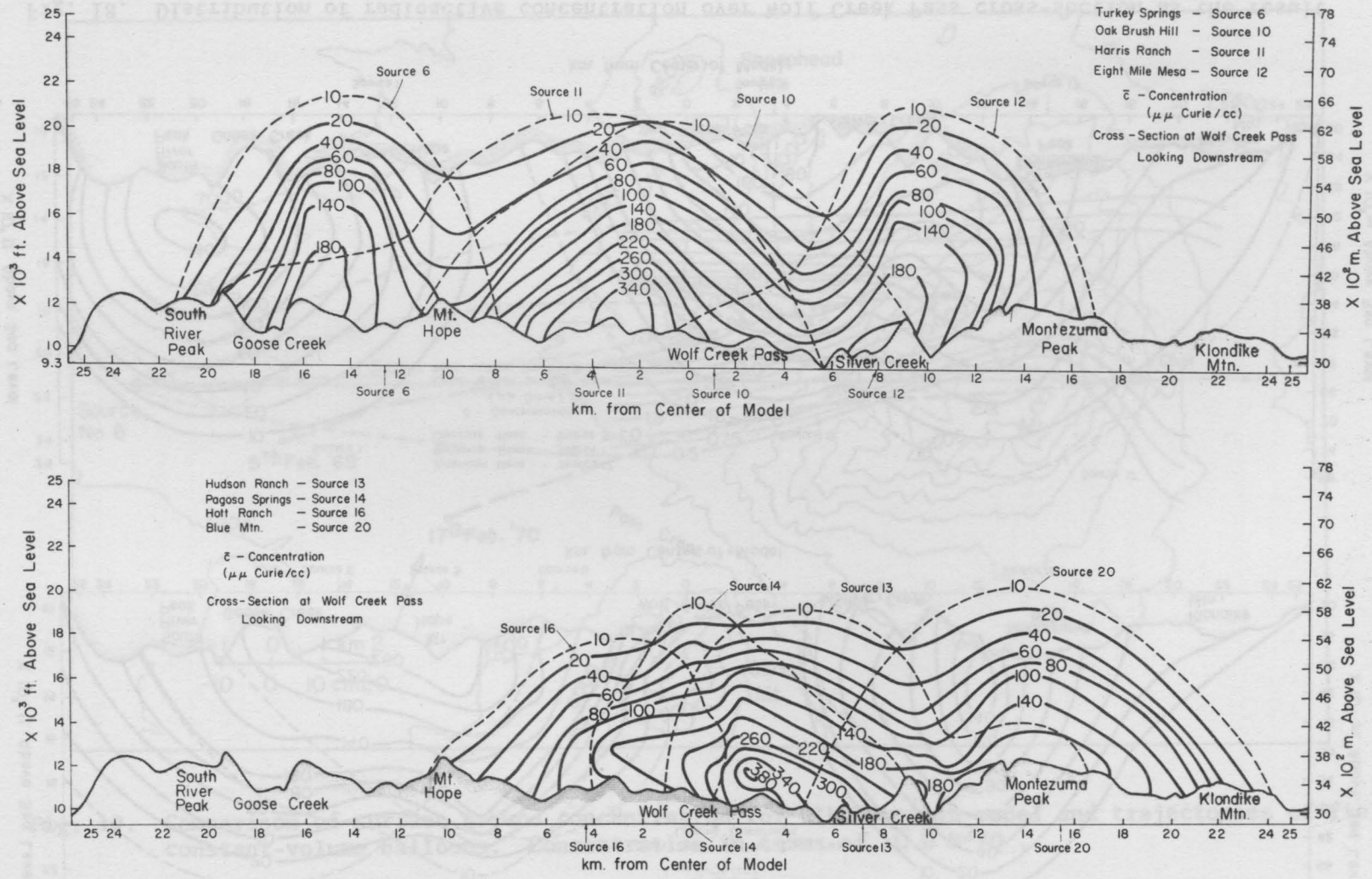

Fig. 17. Distribution of radioactive concentration over Wolf Creek Pass cross-section as the result of multiple sources.

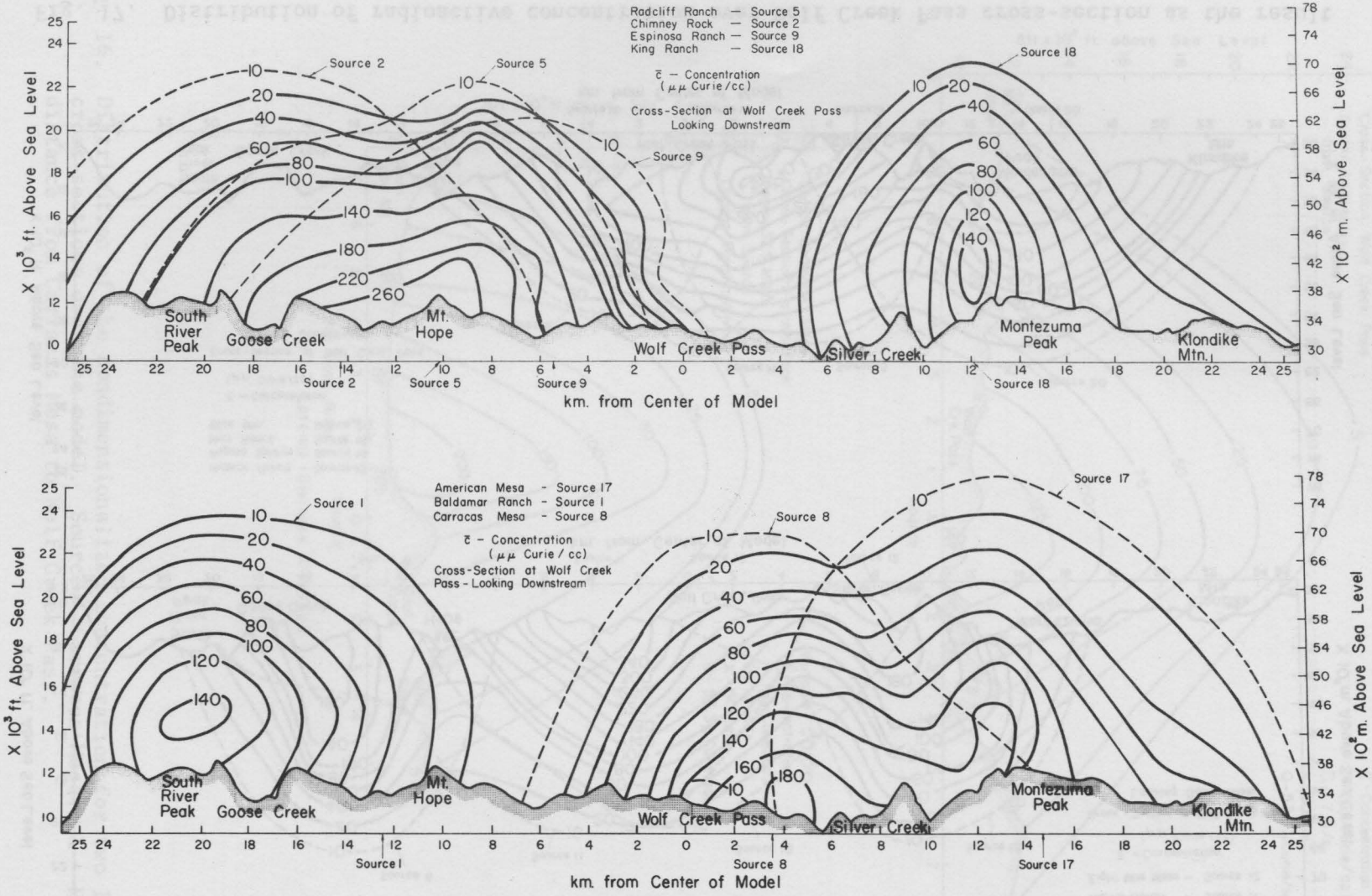

Fig. 18. Distribution of radioactive concentration over Wolf Creek Pass cross-section as the result of multiple sources.

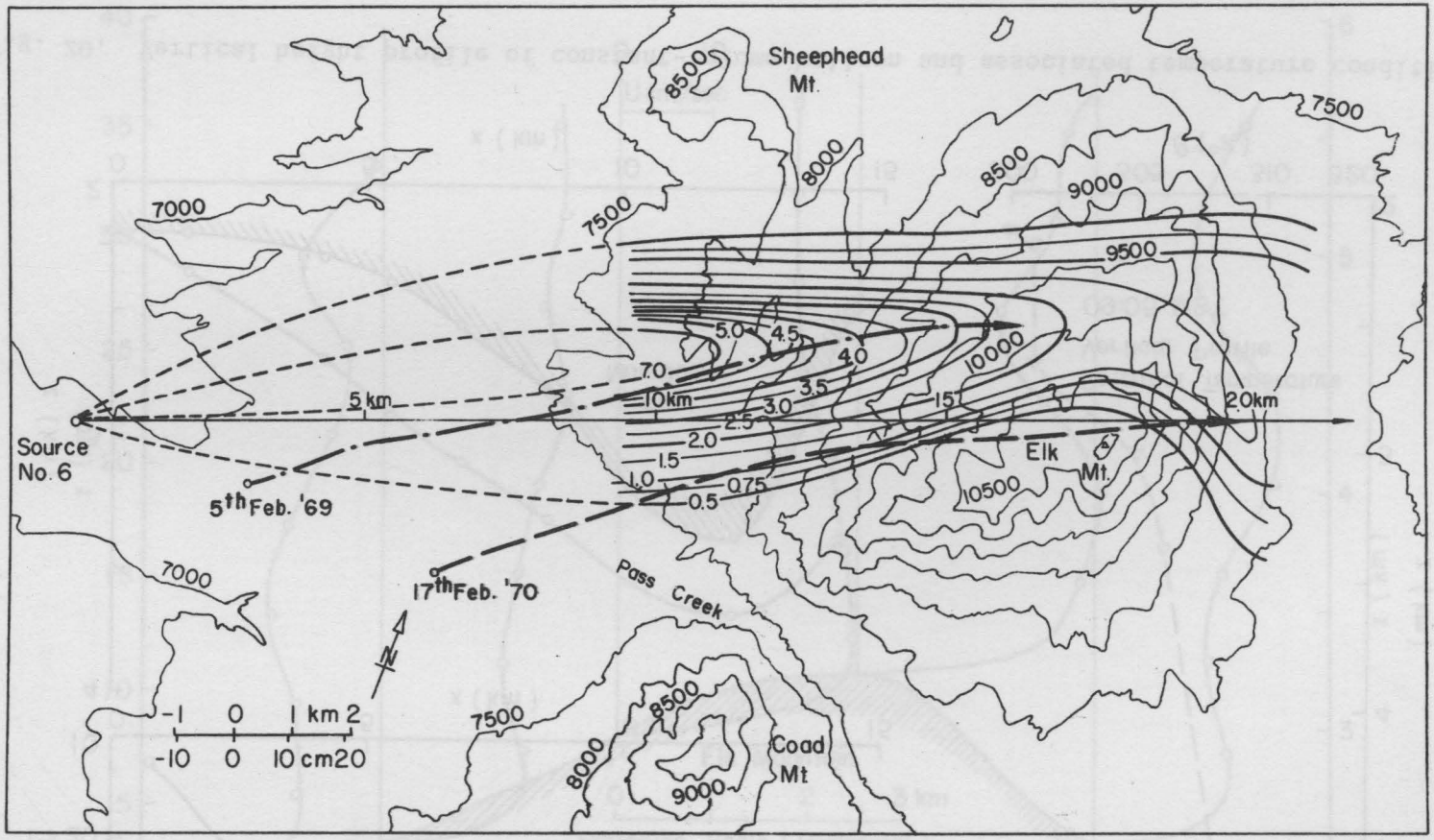

Fig. 19. Comparison of surface ground concentration for Elk Mountain model and trajectories of field constant-volume balloons. Concentration in terms of $\overline{C}\,\overline{U}\,H^2/Q$.

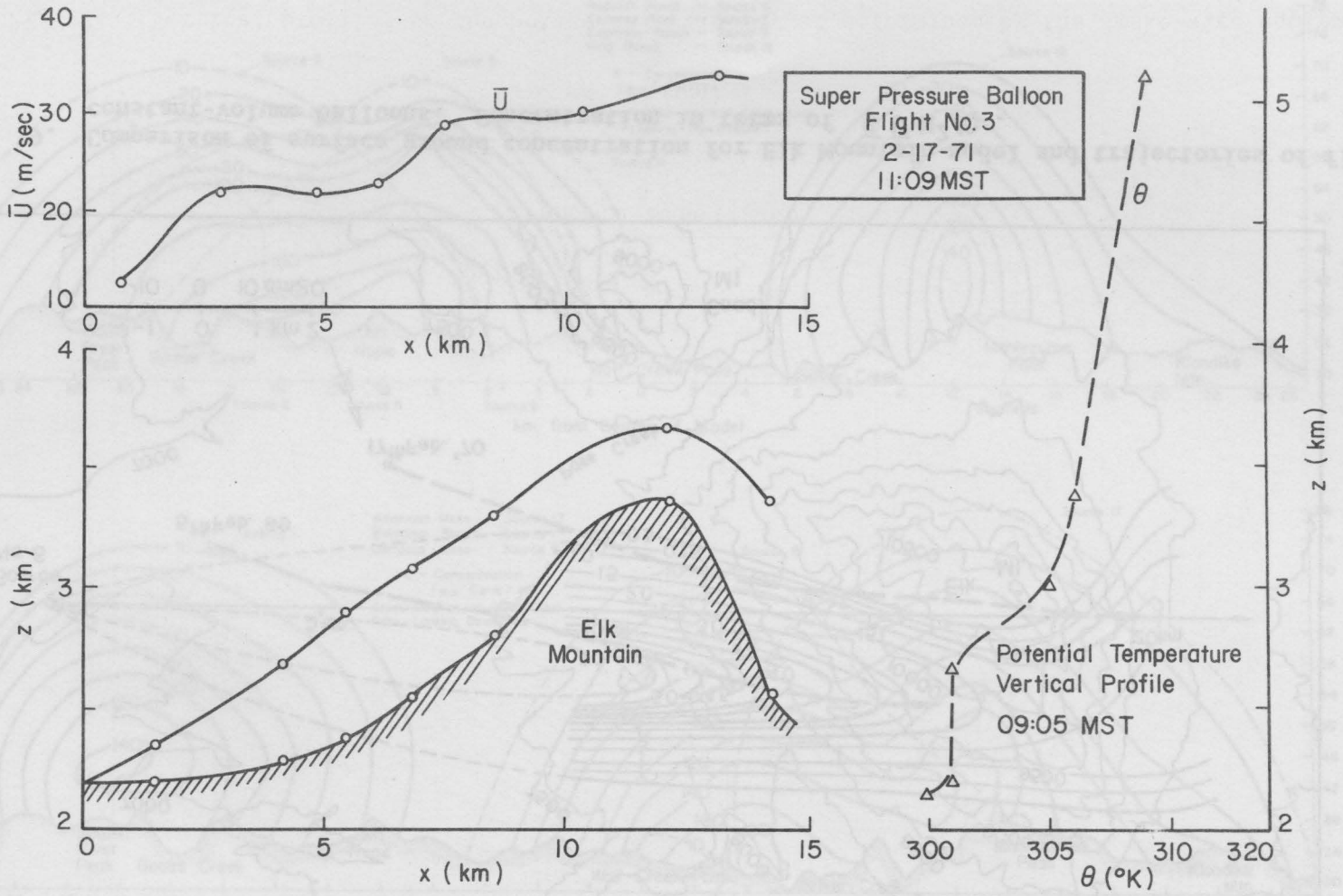

Fig. 20. Vertical height profile of constant-volume balloon and associated temperature conditions.

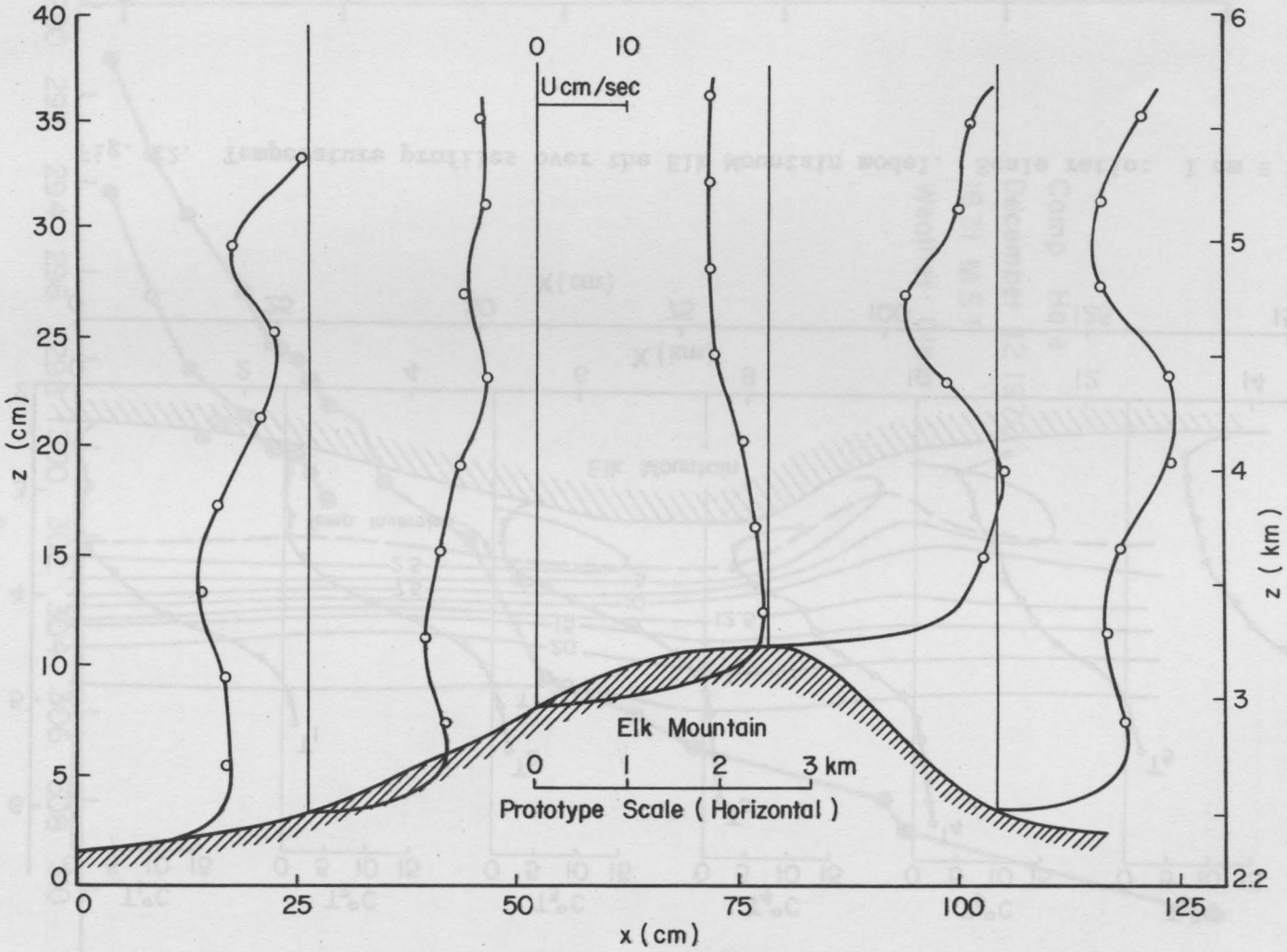

Fig. 21. Vertical profiles of the horizontal velocity as determined by the smoke-wire equipment. Scale ratio: 1 cm ≡ 96 m .

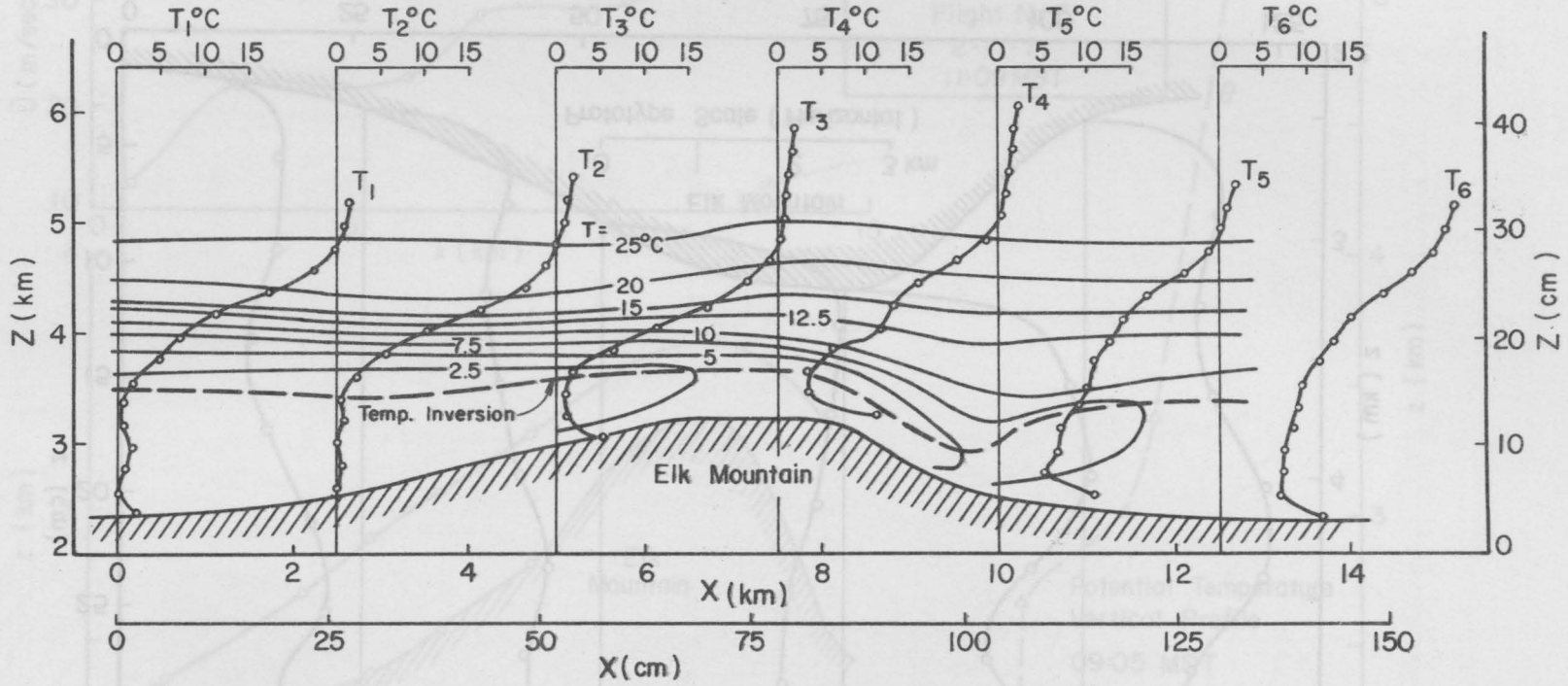

Fig. 22. Temperature profiles over the Elk Mountain model. Scale ratio: 1 cm ≡ 96 m .

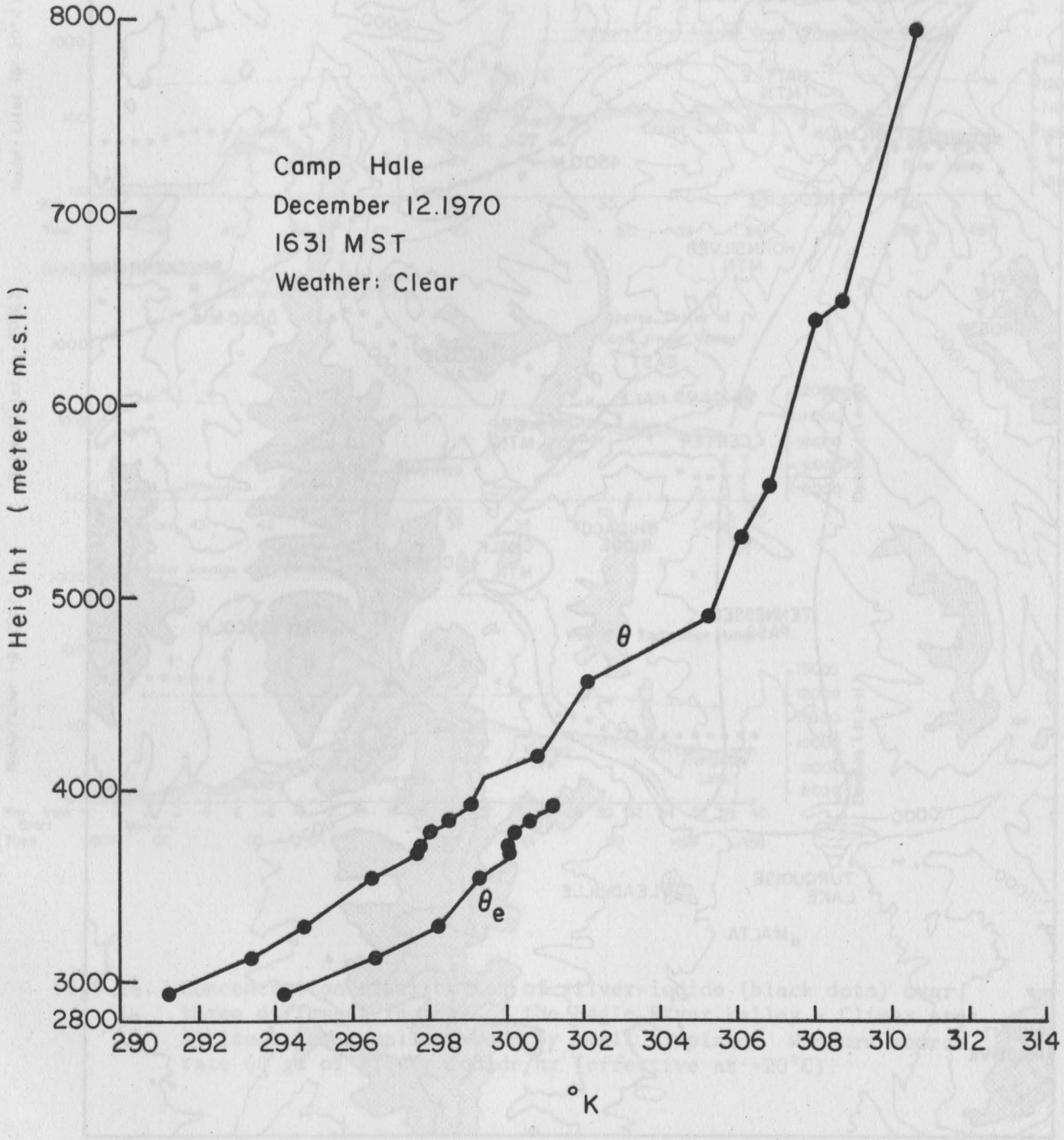

Fig. 23. Potential and equivalent potential temperature profile at Camp Hale during day of aircraft sampling.

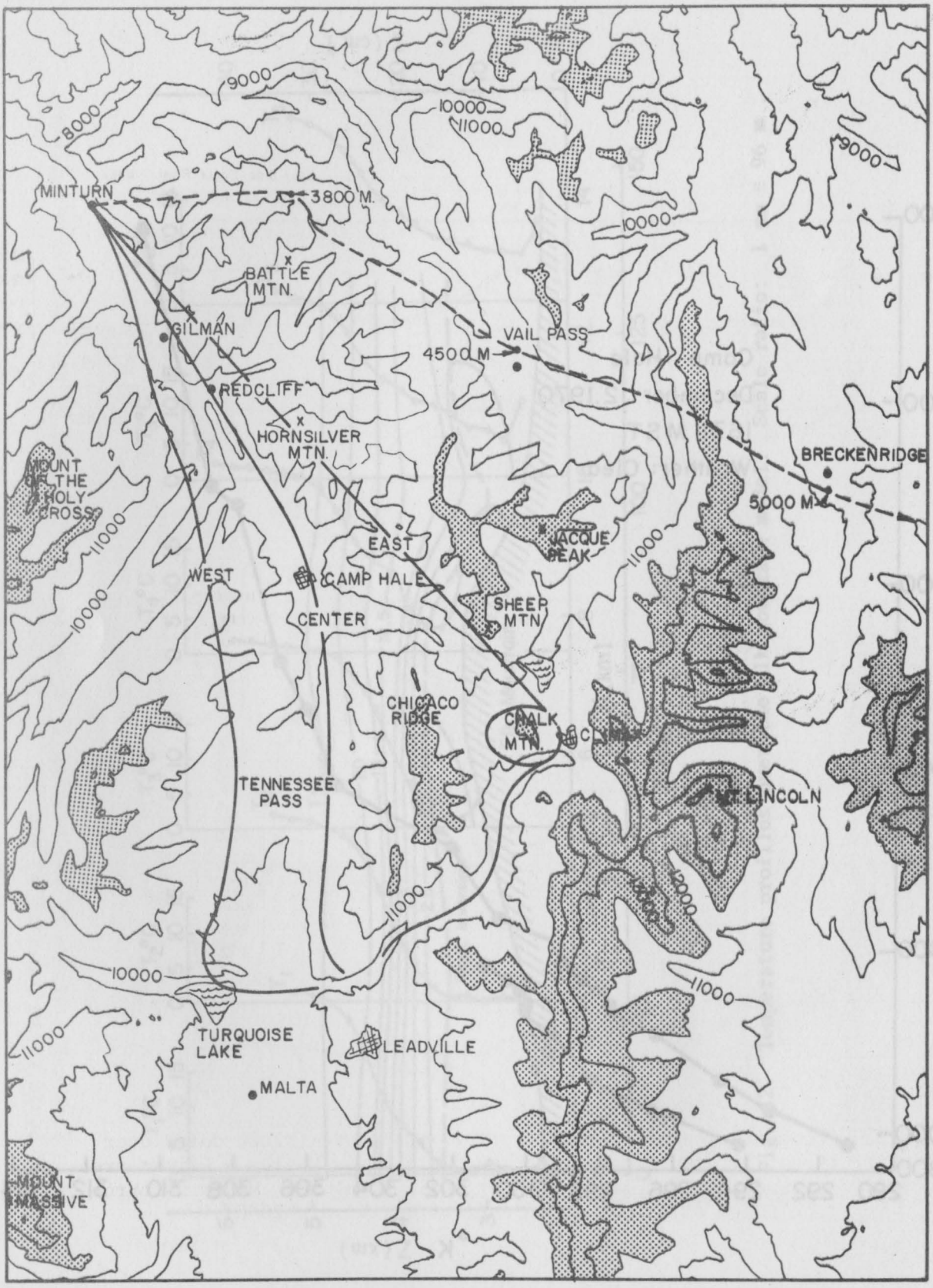

Fig. 24. Constant-volume balloon trajectory (dash line) with altitudes above sea level and aircraft sampling tracks.

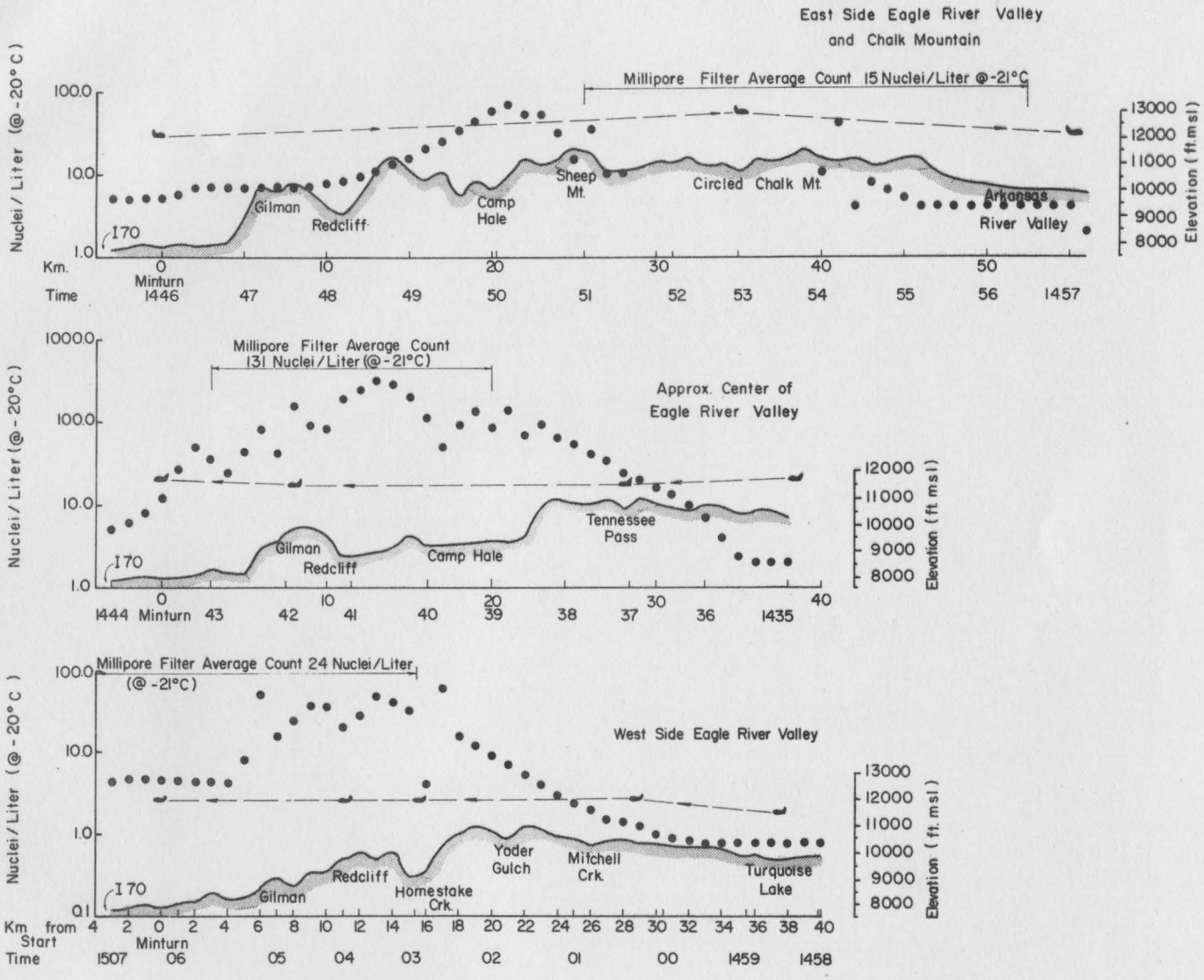

Fig. 25. Concentration distribution of silver-iodide (black dots) over three different regions of the Eagle River Valley - Climax area. Altitudes of sampling shown by small airplane. Minturn source rate 60 gm of silver iodide/hr (effective at -20°C).